

The Physics of Pair Density Waves: Cuprate Superconductors and Beyond

Daniel F. Agterberg,¹ J.C. Séamus Davis^{2,3},
 Stephen D. Edkins⁴, Eduardo Fradkin,⁵ Dale J.
 Van Harlingen⁵, Steven A. Kivelson⁶, Patrick
 A. Lee⁷, Leo Radzihovsky⁸, John M.
 Tranquada⁹, and Yuxuan Wang¹⁰

¹Department of Physics, University of Wisconsin-Milwaukee

²Clarendon Laboratory, Oxford University

³Department of Physics, University College Cork

⁴Department of Applied Physics, Stanford University

⁵Department of Physics and Institute for Condensed Matter Theory, University of Illinois at Urbana-Champaign

⁶Department of Physics, Stanford University

⁷Department of Physics, Massachusetts Institute of Technology

⁸Department of Physics and Center for Theory of Quantum Matter, University of Colorado, Boulder, CO 80309

⁹Department of Physics, Brookhaven National Laboratory

¹⁰Department of Physics, University of Florida

Xxxx. Xxx. Xxx. Xxx. YYYY. AA:1–30

[https://doi.org/10.1146/\(\(please add article doi\)\)](https://doi.org/10.1146/((please add article doi)))

Copyright © YYYY by Annual Reviews.
 All rights reserved

Keywords

keywords, separated by comma, no full stop, lowercase

Abstract

We review the physics of pair density wave (PDW) superconductors. We begin with a macroscopic description that emphasizes order induced by PDW states, such as charge density wave, and discuss related vestigial states that emerge as a consequence of partial melting of the PDW order. We review and critically discuss the mounting experimental evidence for such PDW order in the cuprate superconductors, and the status of the theoretical microscopic description of such order. In addition, we give an overview of the weak coupling version of PDW order, Fulde-Ferrell-Larkin-Ovchinnikov states, in the context of cold atom systems, unconventional superconductors, and non-centrosymmetric and Weyl materials.

Contents

1. INTRODUCTION	2
2. PHENOMENOLOGICAL THEORY	3
2.1. Phenomenological Theory: Ginzburg-Landau-Wilson formulation	3
2.2. Coupling of PDW to uniform superconducting order	6
2.3. Bogoliubov spectrum of a pair density wave	6
3. CUPRATES	8
3.1. $\text{La}_{2-x}\text{Ba}_x\text{CuO}_4$ and related cuprates	8
3.2. $\text{Bi}_2\text{Sr}_2\text{CaCu}_2\text{O}_{8+\delta}$: Vortex Halos and Josephson Microscopy	11
4. OTHER SYSTEMS	13
4.1. Organics, Fe-based superconductors, and heavy fermion materials	13
4.2. Pair Density Wave in degenerate atomic gases: FFLO	14
5. MECHANISM	15
5.1. Evidence of PDW in Models of Strongly Correlated Systems	15
5.2. Fulde-Ferrell-Larkin-Ovchinnikov state in degenerate atomic gases	17
5.3. Nonuniform pairing in non-centrosymmetric and Weyl superconductors	20
6. BROADER RELEVANCE	22

1. INTRODUCTION

A pair density wave (PDW) is a superconducting state in which the order parameter varies periodically as a function of position in such a way that its spatial average vanishes. It is a phase of matter defined in terms of broken symmetries (1, 2, 3, 4, 5, 6, 7). In this review, we characterize the macroscopic properties of such a state precisely, discuss the status of the (incomplete) theoretical understanding of the sorts of lattice-scale interactions that give rise to it (the “mechanism”), how it is distinct from other phases with which it shares certain features, and the way in which the partial melting of the PDW can give rise to daughter phases with a variety of patterns of vestigial order. In addition to its intrinsic interest, there is now suggestive evidence that significant (although probably not long-range correlated) PDW order exists in at least some regions of the phase diagram of the cuprate high temperature superconductors. We critically review this evidence, and then speculate on the broader significance of these sightings to the understanding of broader issues in the physics of the cuprates. We also discuss other strongly correlated systems, including other unconventional superconductors, certain cold atom systems, and carefully engineered mesoscopic devices, in which PDW and PDW-related states play an important role.

In a time-reversal- and inversion-invariant Fermi liquid, the superconducting (SC) susceptibilities $\chi_{sc}(\mathbf{q}, T)$ at $\mathbf{q} = \mathbf{0}$ diverge as the temperature lowers towards a critical value). Under some circumstances, there can be a local maximum in $\chi_{sc}(\mathbf{q})$ at non-zero \mathbf{q} , but it is always smaller than $\chi_{sc}(\mathbf{0})$. Weak breaking of time-reversal symmetry can change the situation. For example, in the presence of a Zeeman magnetic field, the $T \rightarrow 0$ divergence of $\chi_{sc}(\mathbf{0})$ is cut off with the result that the maximum of χ_{sc} can occur at a wavenumber with $|\mathbf{q}| \sim \epsilon_Z/v_F$ where the Zeeman energy is $\epsilon_Z = g\mu_B H$ and v_F is the Fermi velocity. While there is no longer a strict instability to a superconducting state at arbitrary weak interactions, under some circumstances such a system can form a finite \mathbf{q} superconducting phase at low T . This is the long-sought Fulde-Ferrell-Larkin-Ovchinnikov (FFLO) phase (1, 2), which (as we will briefly review) has been plausibly shown to exist in certain materials and cold-atom systems.

On the other hand, it has been conjectured that, for systems in which the interactions are not weak, a PDW could occur independent of any explicit time-reversal symmetry breaking. In that it does not necessarily break time-reversal symmetry, the PDW is thermodynamically distinct from an FFLO state; that the spatial average of the superconducting order vanishes distinguishes the PDW from a less exotic phase with simply coexisting charge density wave (CDW) and SC order. However, while it is straightforward to examine the phenomenological consequences of the existence of a PDW in terms of the standard methods of effective field theory, developing a microscopic theory has proven challenging. It is not favored at weak coupling and a treatment of the strong coupling problem faces obvious challenges. In this review we focus on the phenomenological aspects and comment briefly on the microscopic models in section 5.

Thus, this is less a review of a well-settled subject than a progress report on an interesting, rapidly developing subject. The experimental evidence – especially in the cuprates – is sufficiently dramatic that it cannot be ignored. However, there is not yet the web of consistent evidence from a wide variety of experiments that one would ideally count on to establish the correctness of any particular perspective on the properties of such complex materials. This, combined with the absence of a reliable microscopic theory means that a portion of the discussion is necessarily speculative. On the other hand, it is part of what makes the subject so

exciting.

2. PHENOMENOLOGICAL THEORY

2.1. Phenomenological Theory: Ginzburg-Landau-Wilson formulation

PDW order denotes a state with spatially varying superconducting order that has no uniform superconducting component, meaning its spatial average vanishes. In one of its simplest incarnations, this state has a $\cos(\mathbf{P} \cdot \mathbf{x})$ spatial gap dependence. A state with this spatial dependence was proposed to occur in the cuprate superconductors as an explanation of experimentally observed suppression of the c -axis Josephson effect (or dynamic layer decoupling) in $\text{La}_{2-x}\text{Ba}_x\text{CuO}_4$ and similar materials (8), reviewed in section 3. Such a cuprate PDW state has a short periodicity, on the order of a few lattice spacings. A state of this form was also originally proposed by Larkin and Ovchinnikov as a superconducting state that emerges when a Zeeman-like magnetic field is applied to a usual, weak-coupling, spin-singlet superconductor (2, 1). In this context, it has been well studied, together with its counterpart Fulde-Ferrell (FF) $e^{i\mathbf{P} \cdot \mathbf{x}}$ state, with a large emphasis on its mean-field stability and on the corresponding electronic excitation spectrum (9, 10). The FFLO-like PDW states qualitatively differ from the cuprate PDW states in two key aspects. The first, due to the Zeeman field, is that they emerge from a broken time-reversal symmetric normal state. The second difference is that they exhibit much longer periodicities, on the order of multiple superconducting coherence lengths, than the cuprate PDW states. It is likely for this reason that the role of other induced orders by the primary FFLO-like PDW order has not been emphasized in the literature. However, such induced orders play an important role in the context of cuprate PDW states and so is reviewed here.

In general, a PDW state has secondary orders whose existence is dictated by symmetry. These induced orders have played an important role in understanding the relevance of PDW order in the cuprates (4, 5, 6, 11, 7, 12, 13, 14, 15). Primary among these is charge density wave (CDW) order: as discussed later, key experimental evidence for PDW order in BSSCO relies on the observation CDW order in the vortex core halo (15). The unidirectional state will exhibit an induced CDW order, this unidirectional PDW state also has nematic and spatially uniform charge $4e$ superconducting orders. These induced order parameters can develop long range order when the original PDW order does not, the induced order is then often called vestigial order (16). Observation and understanding of this induced order is central to understanding the underlying PDW state. In this section, using a Ginzburg-Landau-Wilson (GLW) approach, we illuminate different types of PDW ground states, the accompanying induced order, and the topological excitations of these states. Since the PDW order breaks translation symmetry in addition to the usual gauge symmetry, the topological excitation spectrum is richer than in usual superconductors. Key to this section is that we assume the existence of an underlying lattice that breaks rotational symmetry. This condition is not true in the context of cold atoms and this gives rise to different physical properties which are discussed in section 5.

To be concrete, motivated by the cuprates, we consider a tetragonal system with square lattice sheets stacked along the z -axis. We will consider PDW order that exhibits spatial modulations along the in-plane \hat{x} direction. The modulations will be assumed to be incommensurate with the lattice. Tetragonal symmetry dictates that the PDW order parameter has four complex degrees of freedom with momenta $\pm\mathbf{P}_x$ and $\pm\mathbf{P}_y$, the corresponding order parameter is written as $\Delta_{\mathbf{P}} = \{\Delta_{\mathbf{P}_x}, \Delta_{\mathbf{P}_y}, \Delta_{-\mathbf{P}_x}, \Delta_{-\mathbf{P}_y}\}$. These order parameters are coupled to fermions via

$$H_{\mathbf{P}} = \Delta_{\mathbf{P}} \int d\mathbf{k} F(\mathbf{k}) c_{\mathbf{k}+\mathbf{P}/2}^\dagger c_{-\mathbf{k}+\mathbf{P}/2}^\dagger \quad 1.$$

where $F(\mathbf{k})$ is an internal form factor. Note that the form factor is not a representation of a symmetry group and different form factors, e.g. s -wave, d -wave, can mix (13). Here, for concreteness, we take a s -wave form factor, so that $\Delta_{\mathbf{P}} = \sum_{\mathbf{k}} g \langle c_{-\mathbf{k}\downarrow} c_{\mathbf{k}+\mathbf{P}\uparrow} \rangle$ (where g is the interaction constant) since different form factors do not alter the essential results discussed in this section, as discussed in Ref. (17). To develop the GLW theory, the role of symmetry operations on these order parameters is required. Here we do not write all such symmetry operations and refer to Ref. (17) for a more detailed discussion of these. However, it is worthwhile highlighting some key symmetries that help to understand the additional orders that are induced by the PDW order. In particular, under a lattice translation \mathcal{T} , the PDW order transforms as $\Delta_{\mathbf{P}} \rightarrow e^{i\mathcal{T} \cdot \mathbf{P}} \Delta_{\mathbf{P}}$. Under time-reversal (\mathcal{T}) and parity (\mathcal{P}) symmetries we have:

$$\Delta_{\mathbf{P}} \xrightarrow{\mathcal{T}} (\Delta_{-\mathbf{P}})^* \quad \Delta_{\mathbf{P}} \xrightarrow{\mathcal{P}} \Delta_{-\mathbf{P}}. \quad 2.$$

The GLW energy density consistent with time-reversal, parity, space group, and gauge symmetries is (5, 16)

$$\begin{aligned} \mathcal{H} = & \alpha \sum_i |\Delta_{\mathbf{P}_i}|^2 + \beta_1 (\sum_i |\Delta_{\mathbf{P}_i}|^2)^2 + \beta_2 \sum_{i < j} |\Delta_{\mathbf{P}_i}|^2 |\Delta_{\mathbf{P}_j}|^2 + \beta_3 (|\Delta_{\mathbf{P}_x}|^2 |\Delta_{-\mathbf{P}_x}|^2 \\ & + |\Delta_{\mathbf{P}_y}|^2 |\Delta_{-\mathbf{P}_y}|^2) + \beta_4 [\Delta_{\mathbf{P}_x} \Delta_{-\mathbf{P}_x} (\Delta_{\mathbf{P}_y} \Delta_{-\mathbf{P}_y})^* + (\Delta_{\mathbf{P}_x} \Delta_{-\mathbf{P}_x})^* \Delta_{\mathbf{P}_y} \Delta_{-\mathbf{P}_y}]. \end{aligned} \quad 3.$$

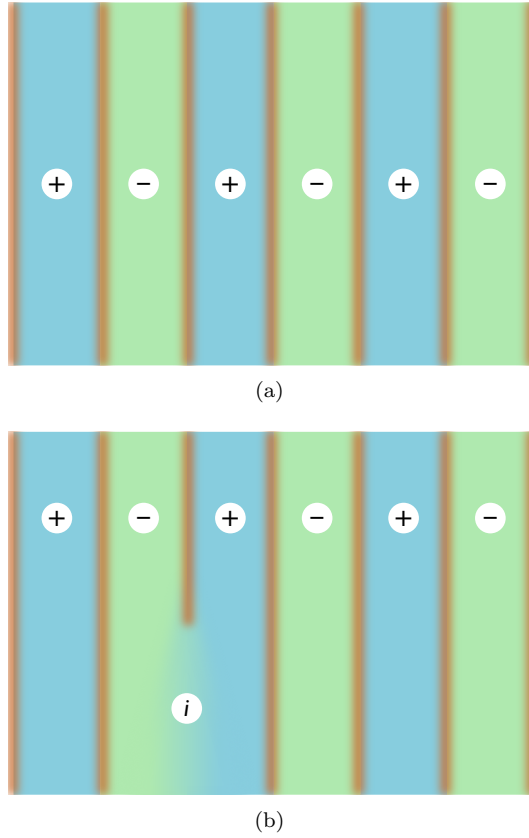


Figure 1

Panel (a): Schematic real-space illustration of a unidirectional PDW state (blue and green stripes) with $\Delta_{\pm\mathbf{P}}$ its induced CDW state (orange stripes) $\rho_{\mathbf{Q}=2\mathbf{P}}$. The PDW order parameter change sign in alternate domains and vanishes at the domain walls, while the local density of states is enhanced at the domain walls. The local density of state has a CDW pattern with half the wavelength of the PDW. Panel (b): The PDW half vortex, around which the local SC phase winds by π , bound with a CDW dislocation.

Phase	$(\Delta_{\mathbf{P}_x}, \Delta_{\mathbf{P}_y}, \Delta_{-\mathbf{P}_x}, \Delta_{-\mathbf{P}_y})$	Induced Orders
FF-type	$(e^{i\phi_1}, 0, 0, 0)$	$l_x, \epsilon_{x^2-y^2}$
FF*-type	$(e^{i\phi_1}, e^{i\phi_2}, 0, 0)$	$l_x = l_y$
Unidirectional	$(e^{i\phi_1}, 0, e^{i\phi_2}, 0)$	$\rho_{\mathbf{P}_x-\mathbf{P}_y}, M_{\mathbf{P}_x-\mathbf{P}_y}^z$
		$\epsilon_{x^2-y^2}, \Delta_{4e}$
Bidirectional-I	$(e^{i\phi_1}, e^{i\phi_2}, e^{i\phi_3}, e^{i[\phi_1+\phi_3-\phi_2]})$	$\rho_{2\mathbf{P}_x}$
		Δ_{4e}
Bidirectional-II	$(e^{i\phi_1}, ie^{i\phi_2}, e^{i\phi_3}, ie^{i[\phi_1+\phi_3-\phi_2]})$	$\rho_{2\mathbf{P}_x}, \rho_{2\mathbf{P}_y}, \rho_{\mathbf{P}_x-\mathbf{P}_y}, \rho_{\mathbf{P}_x+\mathbf{P}_y}$
		Δ_{4e}
		$\rho_{2\mathbf{P}_x}, \rho_{2\mathbf{P}_y}, M_{\mathbf{P}_x-\mathbf{P}_y}^z, M_{\mathbf{P}_x+\mathbf{P}_y}^z$

Table 1 PDW Ground States. Distinct PDW ground states and accompanying induced orders. In the third column, other modes can be found by using the relationships $\rho_{\mathbf{Q}} = (\rho_{-\mathbf{Q}})^*$ and $M_{\mathbf{Q}}^z = (M_{-\mathbf{Q}}^z)^*$.

The parameters β_i depend upon the specific microscopic model. Depending on which values are found for these, one of five possible ground states can be realized. These five phases are: the FF-type phase with only one momentum component, the FF* phase which is a bidirectional version of the FF-type phase, the LO type which include pairing with opposite momentum components: these include the unidirectional phase, and Bidirectional-I (II) phase which has a phase factor of 0 ($\pi/2$) between the two unidirectional components. These five states give rise to different patterns of induced order, providing a means to distinguish them. We now turn to these induced orders.

Induced Order Parameters

PDW order can break many symmetries, for this reason it gives rise to a variety of induced orders associated with these broken symmetries. These orders include CDW order ($\rho_{\mathbf{Q}}$) associated with broken translation symmetry (5, 6, 7, 18), magnetization density wave (MDW) order ($M_{\mathbf{Q}}^z$) associated with broken time-reversal and translation symmetries (5, 7), Ising nematic order ($\epsilon_{x^2-y^2}$) associated with broken rotational symmetry (6, 18), loop-current order (l_i) associated with broken time-reversal and parity symmetries (12), and translation invariant charge-4e superconducting order (Δ_{4e}) associated with broken gauge symmetry (18, 11). The induced

orders appearing in the different PDW ground states are shown in Table 1. We now look at these induced orders in more detail.

In the context of the cuprates, Ising nematic and CDW order have been the most important of the induced orders. Since the induced CDW order appears often in this review, we discuss it first. CDW order preserves time-reversal and breaks translation symmetry and, given two superconducting order parameters with different pair density momenta, the CDW order is generally induced as

$$\rho_{\mathbf{P}_i - \mathbf{P}_j} \propto (\Delta_{\mathbf{P}_i} \Delta_{\mathbf{P}_j}^* + \Delta_{-\mathbf{P}_j} \Delta_{-\mathbf{P}_i}^*) \quad 4.$$

where the second term follows from time-reversal invariance. Two important examples of this are i) in the unidirectional PDW state $\rho_{2\mathbf{P}} \propto \Delta_{\mathbf{P}} \Delta_{-\mathbf{P}}^*$ (see Fig. 1(a) for a real space illustration; note time-reversal symmetry transforms this term into itself) and ii) when one of the superconducting order parameters is translation invariant, then $\rho_{\mathbf{P}} \propto (\Delta_0 \Delta_{-\mathbf{P}}^* + \Delta_{\mathbf{P}} \Delta_0^*)$ where Δ_0 is a usual translation invariant superconducting order. The PDW ground states that are most often discussed with respect to the cuprates are the unidirectional and the bidirectional-II PDW states. This is because these states exhibit CDW order at momentum $2\mathbf{P}_x$ and none at momentum $\mathbf{P}_x + \mathbf{P}_y$, which is consistent with experiment.

Now we turn to the other induced orders. Ising nematic order which breaks rotational 4-fold symmetry is given by $\epsilon_{x^2-y^2} \propto (|\Delta_{\mathbf{P}_x}|^2 + |\Delta_{-\mathbf{P}_x}|^2 - |\Delta_{\mathbf{P}_y}|^2 - |\Delta_{-\mathbf{P}_y}|^2)$. MDW order, which arises from spatially modulated orbital loops currents is given by $M_{\mathbf{P}_i - \mathbf{P}_j}^z \propto i(\Delta_{\mathbf{P}_i} \Delta_{\mathbf{P}_j}^* - \Delta_{-\mathbf{P}_j} \Delta_{-\mathbf{P}_i}^*)$. Translation invariant charge-4e superconducting order is given by $\Delta_{4e} \propto \Delta_{\mathbf{P}} \Delta_{-\mathbf{P}}$. Uniform charge-4e superconducting order, a state with $hc/4e$ flux quantization, can occur if the CDW stiffness of the PDW state is sufficiently weak (11), or in continuum systems (where the stripe order melts at any temperature) (19, 20). It may also arise in PDW states with quench disorder (21). Loop current order, which is odd under both time-reversal and parity symmetries, but preserves translation symmetry is given by $l_i \propto (|\Delta_{\mathbf{P}_i}|^2 - |\Delta_{-\mathbf{P}_i}|^2)$.

Topological excitations

Just as gauge invariance of the action implies the existence of vortices in usual superconductors, gauge and translation invariance of the Hamiltonian in Eq. 3. imply topological excitations in PDW superconductors. Due to breaking of translation symmetry, these PDW topological excitations can exhibit properties that are quite different from usual superconducting vortices. This is reflected in the appearance of multiple $U(1)$ symmetries that appear in most PDW ground states. Gauge and translation symmetries allow PDW ground states to have up to three $U(1)$ symmetries (one from usual gauge invariance and one each from translation invariance along the \hat{x} and \hat{y} directions). In Table 1, these $U(1)$ symmetries are given by the phase factors ϕ_i , which are not determined by minimizing the action. These undetermined phases lead to Goldstone modes, in particular new modes associated with translational symmetry breaking. These modes are discussed in more detail in section 5.2. A winding in one or some of these ϕ_i gives rise to the topological excitations.

Physics associated with topological excitations are discussed in detail in Refs. (5, 7, 11, 18). Here we focus on the unidirectional (LO) state, which is sufficient to capture the key new physical properties associated with these vortices. Writing $(\Delta_{\mathbf{P}_x}, \Delta_{\mathbf{P}_y}, \Delta_{-\mathbf{P}_x}, \Delta_{-\mathbf{P}_y}) = \Delta(e^{i\phi_1}, 0, e^{i\phi_2}, 0)/\sqrt{2}$, we allow (ϕ_1, ϕ_2) to have a phase winding of (n, m) times 2π respectively. These we will call (n, m) vortices. These vortices are most simply described by the following London theory

$$\mathcal{H}_L = \frac{1}{2} \sum_{i=x,y,z} \left\{ \rho_{s,i} [(\nabla_i \phi_1 - 2eA_i)^2 + (\nabla_i \phi_2 - 2eA_i)^2] + B_i^2 \right\} \quad 5.$$

where $\rho_{s,i}$ give the superfluid stiffness along these three directions (it is generally anisotropic) and the magnetic field $B = \nabla \times A$. This Eq. 5. gives rise to a supercurrent with components $J_i \propto \rho_{s,i} [\nabla_i(\phi_1 + \phi_2)/2 - 2eA_i]$. Far from the core of the vortex, the minimum energy configuration has zero supercurrent, and a contour integration of this supercurrent then implies that the flux enclosed in a (n, m) vortex is $(n+m)\Phi_0/2$, n and m being the winding number in ϕ_1 and ϕ_2 . Consequently, $(1, 0)$ vortices enclose half the usual flux quantum. (5) In this description, $(1, 1)$ vortices are usual single flux quantum Abrikosov vortices. Eq. 5. shows that these usual superconducting vortices typically have the lowest energy because the phase winding can be completely screened by the vector potential, implying that they have a finite energy per unit length. Fractional or zero-flux vortices have an energy per unit length that diverges as the logarithm of the cross sectional system size.

An examination of the induced CDW order near a $\Phi_0/2$ $(1, 0)$ vortex sheds insight into their physical origin. In particular, the relationship $\rho_{2\mathbf{P}} \propto \Delta_{\mathbf{P}} \Delta_{-\mathbf{P}}^*$ reveals that a dislocation appears in the CDW order due to the phase winding in $\Delta_{\mathbf{P}_x}$. Since this CDW order has half the periodicity of the PDW order, a dislocation in the CDW order corresponds to half a dislocation in the PDW order. Consequently, the half-flux vortex can be seen as a half-dislocation combined with a π phase winding in the PDW order [see Fig. 1(b)]. The $\Phi_0/2$ vortices of the other PDW phases have a similar origin. A generic prediction is that a PDW superconducting vortex containing a half a flux quantum will be pinned to a dislocation in the induced CDW order.

These (n, m) vortices can have some notable physical consequences (5, 7, 11, 18). One example is in fluctuation driven vortex physics in two dimensions (22, 23, 24). In particular, it is possible that the lowest energy vortex is not a $\Phi_0/2$ $(1, 0)$ vortex but either a $(1, 1)$ Abrikosov vortex or a $(1, -1)$ PDW dislocation. At a vortex unbinding transition, the lowest energy vortices will proliferate, leading to a phase that no longer has PDW order, but has vestigial order in one of the induced order parameters. In the case that the $(1, 1)$ Abrikosov vortices proliferate (these can be the lowest energy vortices due to the presence of the vector potential), the resultant phase will have only CDW order with wavevector twice the PDW wavevector (5). In the case that $(1, -1)$ PDW dislocations proliferate, the resultant phase will be a charge $4e$ superconductor (11, 18). As discussed in section 5.2, this case is particularly relevant in the context of cold atoms due to rotational symmetry.

2.2. Coupling of PDW to uniform superconducting order

The interpretation of a key cuprate experimental result (15) in the context of PDW order requires an understanding of the coexistence of PDW order with usual superconducting d-wave order (Δ_d). Here we present the simplest coexistence term that allows this to be addressed in zero magnetic field (an extension to finite field will be discussed later). In zero field, the lowest order coupling term is given by

$$\begin{aligned} \mathcal{H}_c = & \beta_{c1} \sum_i |\Delta_d|^2 |\Delta_{\mathbf{P}_i}|^2 + \beta_{c2} [\Delta_d^2 (\Delta_{\mathbf{P}_x} \Delta_{-\mathbf{P}_x} + \Delta_{\mathbf{P}_y} \Delta_{-\mathbf{P}_y})^* \\ & + (\Delta_d^2)^* (\Delta_{\mathbf{P}_x} \Delta_{-\mathbf{P}_x} + \Delta_{\mathbf{P}_y} \Delta_{-\mathbf{P}_y})]. \end{aligned} \quad 6.$$

A key feature of this coupling is that the β_{c2} term can always be made negative by the correct choice of the relative phases between the PDW and d-wave orders. This has two consequences, the first is that this coupling prefers the unidirectional (LO) or bidirectional-I PDW states. The second relates to the observation that coexisting PDW and uniform d -wave orders imply either the appearance of CDW $\rho_{\mathbf{P}}$ or MDW $M_{\mathbf{P}}^z$ order at the *same* momentum as the PDW order. Whether it is CDW or MDW order depends upon the sign of the coefficient β_{c2} , if this is positive, then MDW will appear, if it is negative then CDW order will appear. Note that the coupling term β_{c2} locks the phase of the uniform Δ_d order to the unidirectional (LO) and bidirectional PDW phases, consequently, half-flux quantum vortices will not longer exist. Note that even if in the ground state Δ_d and $\Delta_{\mathbf{P}}$ do not coexist due to their competition, it is still possible that they coexist near vortices of either order, where the ground state order parameter is locally suppressed. We refer the reader to Sec. 3.2 for a review of recent experimental evidence of PDW near SC vortex halos.

There are two aspects that were not discussed here but deserve some attention. The first is the phenomenological response of the PDW order to static impurities and the second is the consequence of commensurate PDW order. Non-magnetic impurities do not couple directly to the PDW order but couple to the induced CDW order (6, 21). The primary consequence of this is that for weak disorder, one expects a destruction of the PDW order, resulting in vestigial order in the Δ_{4e} and that the induced CDW order will be disordered on the Imry-Ma length scale (21). In addition, disorder can locally nucleate induced orders that do not generically appear in the PDW ground state of interest (25). In contrast to the above considerations for incommensurate PDW order, in a PDW commensurate with the lattice potential, the latter gaps out the PDW phonons (the $\phi_1 - \phi_2$ mode), thereby precluding half-vortex defects (5).

2.3. Bogoliubov spectrum of a pair density wave

Next we review some properties of the Bogoliubov spectrum associated with a PDW and point out a number of features which makes it distinct from uniform pairing. As an illustration we initially discuss what happens to the Cuprate band structure if we impose a unidirectional PDW order with $\Delta_{\mathbf{P}_x}, \Delta_{-\mathbf{P}_x}$ on it.

In Fig 2, we pair electrons with momenta \mathbf{p} and $2\mathbf{K} - \mathbf{p}$ to form a PDW with momentum $\mathbf{P}_x = 2\mathbf{K}$ and similarly for $-\mathbf{P}_x$. In this figure \mathbf{K} was chosen to be at the Fermi surface, but the features we discuss will be similar if \mathbf{K} moves away from the Fermi surface. Fig 3 shows a cut of the spectrum at $k_y = \pi$ and the solid black line shows the electron band $\epsilon(\mathbf{k}_x)$. We illustrate the formation of the Bogoliubov spectrum with the usual “semiconductor” representation where the dashed line represent the hole spectrum $-\epsilon(-\mathbf{k}_x + \mathbf{P}_x)$. The hybridization of the two bands form the blue, green and red bands. We can estimate the weight of these bands in a photo-emission experiment by tracking how much of the original solid black band is admixed. For example, the red band is made up mainly of hole bands and will be almost invisible in ARPES. The first thing to note is that unlike the uniform superconductors, the spectrum is not particle hole symmetric. This is due to the shift of the hole band by \mathbf{P}_x . An immediate consequence of this is that the top of the green band does not line up with the Fermi momentum k_F . Fig 4 shows a number of scans for different k_y in an experiment performed in Bi-2201. (26) This material is unique in that there is a quite clear onset of the pseudogap at about 140K while the superconducting T_c is rather low, so that the spectrum can be mapped out over a wide

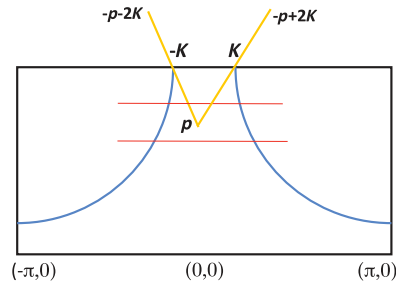


Figure 2

A sketch of the top half of the Brillouin zone for the Cuprates with the Fermi surface shown in blue. Pairing of the electrons as indicated form PDW's with momenta $\pm 2\mathbf{K}$ after Umklapp.

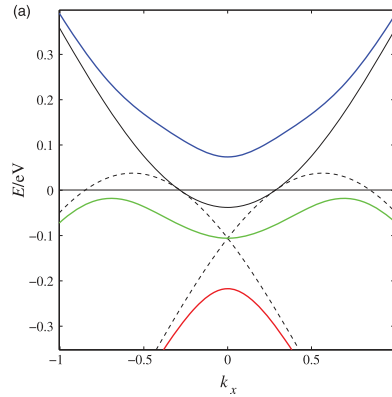


Figure 3

A “semiconductor” picture of the formation of the Bogoliubov band as a function of k_x for $k_y = \pi$. Solid black line is the original electron dispersion. Dashed lines are the hole bands. Note the shift by the PDW momenta by $\pm \mathbf{P}_x$. The blue, green and red lines are the resulting hybridized Bogoliubov bands. From Ref. (7)

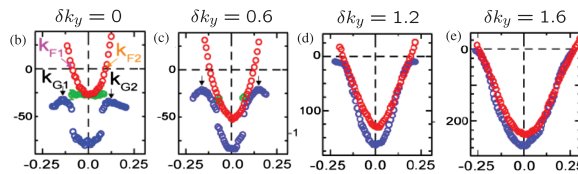


Figure 4

Plots of the ARPES spectra as a function of k_x for several k_y measured from π . The red data points are taken in the high temperature metallic state. The blue data are in the pseudogap phase and the green dots represent additional features that appeared below the superconducting T_C . From Ref. (26).

temperature range covering the high temperature metallic phase, the pseudogap phase and the SC phase. An important point noticed by the experimentalists is that in the scan for $k_y = \pi$, the top of the low temperature band marked by K_G does not line up with the Fermi momentum K_F observed a higher temperature. This was used as an argument against a fluctuating pairing phase as the origin of the pseudogap, but now we see that this objection does not apply to the PDW. Nevertheless, it is worth noting that upon averaging over k space to compute the spectrum which is observed by STS experiments, an approximate particle-hole symmetry can be restored.

A second important observation is that the PDW spectrum naturally has lines of gapless excitations in 2D. This is in contrast with the uniform SC which can only have nodal points in 2D. While these lines of zero's form closed contours, ARPES is dominated by the electron like segments which resembles a line of zero crossing. This is commonly referred to as “Fermi arcs” and was first discovered by ARPES experiments in the pseudogap regime. The existence of these arc-like feature in the PDW spectrum was pointed out by Baruch and Orgad (27) and by Berg et al (6). Here we explain in a bit more detail how it comes about. Returning to Fig. 3 and imagine gradually moving away from $k_y = \pi$, following the scans indicated by the horizontal lines in Fig. 2. The black line in Fig. 3 will move down in energy, but the dashed line will move up. Upon

hybridization the top of the green line moves up in energy and eventually cross zero, resulting in a gapless excitation. With further decrease of k_y from π these crossings continue and form a closed contour of zero crossings, Most of the electron spectral weight lies on the crossing for k_x closer to the origin. This results in the Fermi arc shown in Fig. 5, the back side of the closed loop having almost no weight and is invisible. Here the arc has been symmetrized assuming the co-existence of PDW along both the P_x and P_y directions.

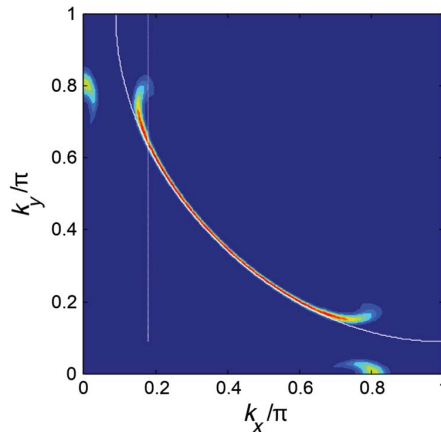


Figure 5

A picture of the Fermi arc of gapless excitations in the PDW state. From Ref. (7).

Finally, let us look in a bit more detail at how the zero crossings appear at the ends of the Fermi arc. From our discussion above it is clear that in the PDW spectrum the zero crossing is formed by an occupied band moving up in energy to meet the Fermi level. This is also what is seen experimentally in Fig. 4. Another candidate for the pseudogap is a CDW at momentum \mathbf{Q} . While this can certainly open a gap at the anti-node near $(0, \pi)$, the gap sits at a fixed momentum k_x and as k_y moves away from π , the occupied states only move to lower energy and remains occupied. Therefore the only way a Fermi arc of gapless excitation can form is for an unoccupied state to move down in energy. This contrasting behavior between a PDW and CDW driven anti-nodal gap and Fermi arc was emphasized in Refs. (6, 7). We also point out that if the PDW is bi-directional and the effect of a composite bi-directional CDW of the type discussed in the last section is added, the Fermi arcs can be connected by the CDW's momenta to form electron-like closed Fermi pockets (7, 14). This mechanism to produce an electron pocket that can explain what is seen in quantum oscillations was first proposed by Harrison and Sebastian. (28) The advantage of the PDW picture is that the hole pockets that remain near the anti-nodes in their picture are automatically gapped-out. Similar features in the Bogoliubov spectrum were obtained with a different version of the PDW state (29), indicating the robustness of the PDW interpretation of the ARPES spectra. A recent paper studied the spectrum of the PDW in a $t - t' - J$ model using the self-consistent Gutzwiller approximation, and reached similar conclusions (30).

In summary, the Bogoliubov spectrum associated with the PDW has a number of features which stand in strong contrast to our intuition based on that of the uniform SC. These include the lack of particle-hole symmetry in the spectrum and nodal lines (surfaces) in two (three) dimensions. In the context of Cuprate superconductors, many of these features are consistent with ARPES results on Bi-2201 which are very difficult to explain based on CDW, fluctuating d-wave SC, or other conventional pictures (26).

3. CUPRATES

3.1. $\text{La}_{2-x}\text{Ba}_x\text{CuO}_4$ and related cuprates

The phase diagram of $\text{La}_{2-x}\text{Ba}_x\text{CuO}_4$, shown in Fig. 6 (LBCO), has an anomalous dip in the bulk superconducting T_c at $x = 1/8$ (31), which is correlated with the appearance of charge and spin stripe orders, as detected by neutron and x-ray diffraction on single crystals (32, 33). Pinning of the stripes to the lattice is enabled by structural distortion within the CuO_2 layers, such that there is a preferred axis along one of the Cu-O directions which rotates by 90° from one layer to the next (34, 35). The relevant distortion appears below a structural phase transition labelled T_{LT} in the figure.

For LBCO with $x = 1/8$, careful measurements of the resistivity within the planes, ρ_{ab} , and perpendicular to the planes, ρ_c , revealed a surprising anisotropy (8, 36). As shown in Fig. 6, cooling below the spin ordering temperature, T_{so} , leads to a drop in ρ_{ab} by an order of magnitude. In contrast, ρ_c continues to rise through T_{so} , eventually turning down at a lower temperature. The drop in ρ_{ab} at ~ 40 K appears to correspond to the

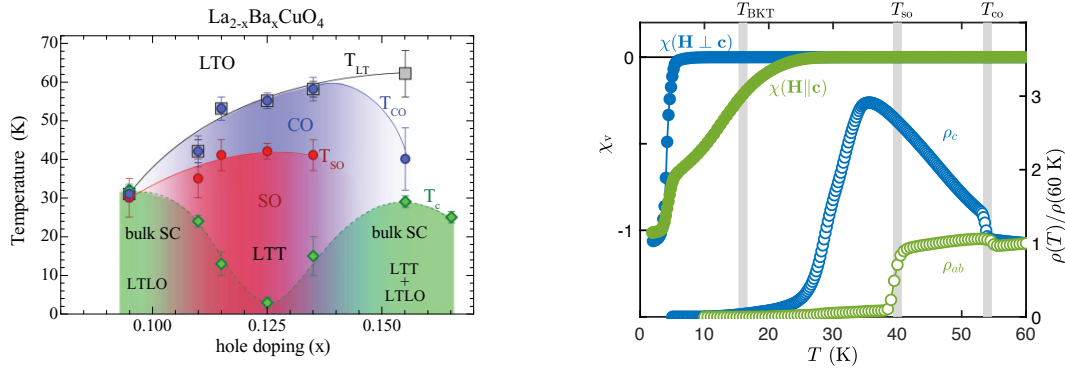


Figure 6

(Left) Phase diagram for $\text{La}_{2-x}\text{Ba}_x\text{CuO}_4$, indicating charge order (CO) below T_{CO} (limited by the structural transition at T_{LT}), spin order (SO) below T_{SO} , and bulk superconductivity (33). (Right) Zero-field-cooled volume susceptibility (left axis, filled symbols) measured with a field of 2 G oriented parallel to the c -axis (probing in-plane screening) and perpendicular to c (probing interlayer screening). In-plane resistivity, ρ_{ab} , and c -axis resistivity, ρ_c , (open symbols, right axis), in $\text{La}_{2-x}\text{Ba}_x\text{CuO}_4$ with $x = 1/8$, replotted from (37, 36).

onset of 2D superconducting correlations within the CuO_2 layers, as confirmed by measurements of anisotropic diamagnetism (36). Below the transition, ρ_{ab} continues to decrease, extrapolating to zero at $T_{\text{BKT}} = 16$ K, where nonlinear transport is observed (8), consistent with a Berezinskii-Kosterlitz-Thouless transition (22, 23); ρ_c remains finite down to ~ 10 K, while bulk susceptibility indicates a bulk superconducting transition at ~ 5 K.

Related behavior is observed in rare-earth-doped $\text{La}_{2-x}\text{Sr}_x\text{CuO}_4$, such as $\text{La}_{1.6-x}\text{Nd}_{0.4}\text{Sr}_x\text{CuO}_4$ (38), associated with the same low-temperature structural phase as in LBCO. In particular, a study of the superconducting state via the c -axis optical reflectivity, measured as a function of Nd concentration (which controls the structural phase and the degree of stripe order), demonstrated a sharp decrease in interlayer Josephson coupling corresponding to the rise of stripe order (39). (At low enough frequency, the layers behave as a coherent superconductor, resulting in a reflectivity of unity. At the frequency of the Josephson plasma resonance (JPR), the interlayer coherence breaks down, and charge oscillates between the layers; the reflectivity drops below the normal-state response before recovering at higher frequency (40).) The JPR results on LNSCO, and the studies of LBCO, motivated proposals that PDW order associated with stripes would cause a cancellation of the interlayer Josephson coupling, consistent with the observation of 2D superconductivity (3, 4).

Somewhat weaker charge stripe (41, 42) and spin stripe (43, 44) order is found in $\text{La}_{2-x}\text{Sr}_x\text{CuO}_4$ with $x \sim 0.12$ in zero field. For $x = 0.10$, it has been observed that applying a c -axis magnetic field induces spin-stripe order (45). Measurements of c -axis reflectivity on a similar sample indicate that the field causes a rapid decrease in the coherent interlayer coupling (46). Similar behavior is found in LBCO $x = 0.095$ (47), where superconductivity in the decoupled planes survives to at least 35 T (48). Evidence for bilayer decoupling has recently been reported for $\text{La}_{2-x}\text{Ca}_{1+x}\text{Cu}_2\text{O}_6$ (49). The field-induced decoupling is similar to the behavior found in LBCO $x = 0.125$, suggesting that PDW order is present in these sample and that it is less sensitive to magnetic field than is the uniform d -wave order.

The loss of coherent coupling between superconducting layers can be explained by the presence of PDW order, but what do other experiments tell us? The superconducting gap for PDW order is predicted, in weak-coupling analysis (27), to be large in the antinodal regions of reciprocal space, but zero along finite arcs centered on the d -wave nodal points. The gap structure can be tested by angle-resolved photoemission spectroscopy (ARPES). Such measurements on LBCO $x = 1/8$ do show the antinodal gap, but they also suggest a d -wave-like dispersion near the nodal region (50, 51). At the node, however, the spectral function is broad in energy and shifted to ~ 20 meV below the chemical potential, similar to a recent observation of a nodal gap in $\text{La}_{2-x}\text{Sr}_x\text{CuO}_4$ with $x = 0.08$ (52). Mean-field calculations of the PDW state that take account of the spin-stripe order predict such a gap (53). While there remains a large degree of uncertainty concerning its interpretation, the ARPES data should not be ignored and will receive further discussion in section 6.

One picture of the PDW state involves superconducting stripes that are phase locked by Josephson coupling. That suggests that optical reflectivity measurements with the polarization in-plane but perpendicular to the stripes might yield a response similar to the JPR behavior found in c -axis reflectivity. Indeed, such behavior has been observed for LBCO $x = 0.125$, with reflectivity approaching one at low frequency and crossing below the normal state response above 20 meV, for temperatures of 40 K and below (54). Another test is to apply a c -axis magnetic field strong enough to destroy the interstripe Josephson coupling. Such an experiment on LBCO $x = 0.125$ finds that, for $T < 1$ K, fields above 30 T are required to eliminate all 2D coherence, resulting

in a highly-resistive metallic state with approximate particle-hole symmetry, consistent with pair correlations surviving in decoupled charge stripes (55).

The cancellation of the Josephson coupling for PDW orders that are orthogonal in adjacent layers applies for linear interactions. If one can drive large ac currents, then it may be possible to induce a nonlinear coupling. Cavalleri's group has demonstrated this on LBCO with x slightly away from $1/8$. For $x = 0.115$, the JPR is at too low an energy to detect; nevertheless, use of a high-intensity THz beam generates a JPR response at the third harmonic, even at temperatures far above the bulk T_c (but below the charge-ordering temperature) (56). This experiment provides intriguing evidence for the PDW state.

One of the most distinctive features of the PDW state is the spatial variation of the order parameter between stripes in the same and adjacent planes. The resulting phase structure in turn suggests several approaches for exploring this exotic phase based on probing the nature of quasiparticle and Josephson tunneling into a PDW material. Several such measurements have been carried out which all exhibit evidence for the predicted PDW phase.

STM on $\text{La}_{2-x}\text{Sr}_x\text{CuO}_4$ $x = 0.12$ with the tunneling current along the c axis revealed an unexpected zero-bias anomaly (57). Subsequent calculations in a t-J model presented an explanation for this observation from a PDW state exhibiting antiphase domains (58). Additional experiments revealed an anisotropic spatial modulation of the zero-bias peak consistent with this model (59).

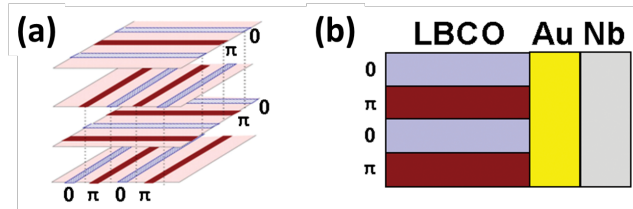


Figure 7

(a) The predicted modulation of the phase of the charge stripes in the PDW state. This can be probed by measuring the current-phase relation of a Josephson junction fabricated between the crystal (LBCO) and a conventional superconductor (Nb), using a Au tunneling barrier.

For a stripe-ordered cuprate such as LBCO, where the interlayer Josephson coupling is frustrated by the orthogonal stripe orientation in neighboring layers [Fig. 7(a)], a proposed test is to reduce the cancellation by applying a magnetic field parallel to the planes; when oriented at 45° to the stripes, the field partially compensates for the momentum mismatch between the layers, causing an enhancement of the Josephson tunneling (60). A test of this type has been done through transport measurements at low temperature and high magnetic field on single crystals of Eu- and Nd-doped $\text{La}_{2-x}\text{Sr}_x\text{CuO}_4$ (61). In a highly dissipative regime with evidence for in-plane superconducting correlations, the ratio of the c -axis to the in-plane resistivity decreased as the in-plane field was increased, consistent with the predicted scenario.

An even more direct test of the PDW state is to probe the Josephson current-phase relation of junctions between the candidate crystal and a conventional superconductor. In the presence of a PDW state, the rapid spatially-modulated sign changes in the Josephson coupling will suppress the first-order Josephson coupling and manifest itself as a significant $\sin(2\phi)$ harmonic in the the current-phase relation of a junction containing LBCO (see Fig. 7b). This phenomenon has been predicted and observed in other junctions with spatially alternating critical current density (62, 63, 64, 65). Additionally, we expect the fraction of Josephson current exhibiting a $\sin(2\phi)$ current-phase relation to increase with T as the interlayer Josephson coupling and conventional 3D superconductivity are suppressed within LBCO, giving way to an increasing proportion of spatially varying 2D superconductivity within the CuO_2 planes (4).

This experiment has recently been carried out by the Van Harlingen group in Urbana on crystals from Genda Gu at Brookhaven (66). Using both dc Josephson interferometry and anisotropic SQUID measurement techniques, they compared the CPR of $\text{La}_{2-x}\text{Ba}_x\text{CuO}_4$ -Au-Nb Josephson junctions for $x = 0.155$ where the T_c is maximum and at $x = 0.125$. As shown in Fig. 8, at $x = 0.155$, the CPR is nearly sinusoidal, with a nearly negligible $\sin(2\phi)$ component. However, at $x = 0.125$, the non-sinusoidal shape of the CPR arising from the onset of a $\sin(2\phi)$ component is apparent. The ratio of the $\sin(2\phi)$ to $\sin(\phi)$ components is observed to increase significantly with temperature as the strength of the superconductivity weakens, consistent with the PDW state. By using junctions fabricated straddling the corner of the crystal, it was also demonstrated that the order parameter symmetry of the crystal remains $d_x^2 - y^2$ in the region where the T_c is suppressed and the PDW state is present.

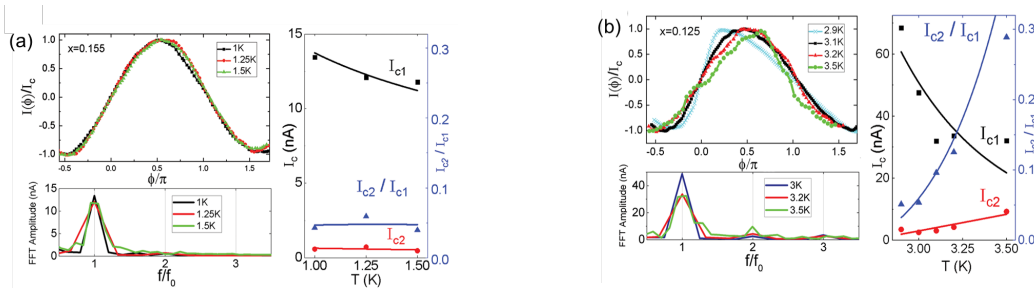


Figure 8

Current-phase relation measurements of $\text{La}_{2-x}\text{Ba}_x\text{CuO}_4\text{-Au-Nb}$ Josephson junctions for (a) $x = 0.155$ where the T_c is maximum and (b) at $x = 0.125$, at the dip in T_c where the PDW state is expected to be strongest. Shown are the shape of the CPR, the FFT spectra extracted from these, and the magnitude of the $\sin(\phi)$ and $\sin(2\phi)$ components and their ratio as a function of temperature. Data obtained with a Josephson junction with the geometry shown in Fig. 7b (from Hamilton et al.(66)).

3.2. $\text{Bi}_2\text{Sr}_2\text{CaCu}_2\text{O}_{8+\delta}$: Vortex Halos and Josephson Microscopy

3.2.1. Spectroscopic Imaging and Josephson STM. Spectroscopic imaging scanning tunnelling microscopy (SISTM) (67) has become a key technique for determining electronic structure of quantum materials. At the surface of each sample, the tip-sample differential conductance for single-electron tunnelling, $\frac{dI}{dV}|_{r,V} \equiv g(\mathbf{r}, E)$, is measured versus voltage $V = \frac{E}{e}$ and location $\mathbf{r} = (x, y)$. The resultant array of $g(\mathbf{r}, E)$ images is related to the density of electronic states $N(\mathbf{r}, E)$ as

$$N(\mathbf{r}, E) \propto \frac{g(\mathbf{r}, E)}{\int^{eV_S} g(\mathbf{r})dE} \quad 7.$$

where V_S is a fixed but arbitrary voltage used to establish each tunnel junction. On the other hand, in Josephson STM the maximum Cooper-pair tunnelling current from a superconducting tip, $I_c(\mathbf{r})$, is measured versus location \mathbf{r} .

3.2.2. Evidence for a PDW in $\text{Bi}_2\text{Sr}_2\text{CaCu}_2\text{O}_{8+\delta}$ in a Magnetic Field. In the of PDW studies, focus has recently turned to modulations of the density of single-electron states $N(\mathbf{r}, E)$ within the vortex halos (68, 69, 70, 71) - regions of suppressed but non-zero superconductivity that surround vortex cores. Whether these modulations stem from a field-induced PDW may be studied using Ginzburg-Landau (GL) analysis. Consider a homogeneous d -wave superconductor $\Delta_{SC}(\mathbf{r}) = F_d \Delta_{SC}$ (where F_d is a d -wave a form factor) coexisting with a uniform PDW $\Delta_{PDW}^P(\mathbf{r}) = F_P \Delta_P [\exp(i\mathbf{P} \cdot \mathbf{r}) + \exp(-i\mathbf{P} \cdot \mathbf{r})]$ with form factor F_{pdw} . The symmetry allowed $N(\mathbf{r})$ modulations generated by interactions occur as products of these two order parameters that transform as density-like quantities. Specifically, the product $\Delta_P \Delta_{SC}^* \Rightarrow N(\mathbf{r}) \propto \cos(\mathbf{P} \cdot \mathbf{r})$ results in $N(\mathbf{r})$ modulations at the PDW wavevector \mathbf{P} , while $\Delta_P \Delta_{-P}^* \Rightarrow N(\mathbf{r}) \propto \cos(2\mathbf{P} \cdot \mathbf{r})$ produces $N(\mathbf{r})$ modulations occurring at $2\mathbf{P}$. Consequently, in the case in which PDW order arises in a halo surrounding a vortex in a d -wave superconductor, there should be two sets of $N(\mathbf{r})$ modulations at \mathbf{P} and at $2\mathbf{P}$ within each halo, with those at $2\mathbf{P}$ decaying with distance from the core at twice the rate as those at \mathbf{P} (if $\Delta_{PDW}^P = \Delta_{PDW}^P(|\mathbf{r}|=0) \exp(-|\mathbf{r}|/\epsilon)$)(12, 13, 14, 15).

To explore these predictions, single-electron tunneling conductance $g(\mathbf{r}, E)$ was measured by Edkins *et al.* (15) for $\text{Bi}_2\text{Sr}_2\text{CaCu}_2\text{O}_{8+\delta}$ samples ($T_c \sim 88\text{K}$; $p \sim 17\%$) at $T = 2\text{K}$. The $g(\mathbf{r}, E)$ is first measured at zero field and then at magnetic field $B = 8.25\text{T}$, in the identical field of view (FOV) using an identical STM tip. The $g(\mathbf{r}, E, B)$ and $g(\mathbf{r}, E, 0)$ are registered to each other with picometer precision, and subtracted to yield $\delta g(\mathbf{r}, E, B) = g(\mathbf{r}, E, B) - g(\mathbf{r}, E, 0)$. This result is the field-induced perturbation to the density of states $\delta N(\mathbf{r}, E, B) \propto \delta g(\mathbf{r}, E, B)$.

Figure 9A shows measured $\delta g(\mathbf{r}, E = 10\text{meV}, B)$ exhibiting the classic 'halo' of modulations in the density of Bogoliubov quasiparticles at $\mathbf{q} \approx [(\pm 1/4, 0); (0, \pm 1/4)] \frac{2\pi}{a_0}$. However, for the energy range $25 < |E| < 50\text{meV}$ which is $|E| \approx \Delta_{SC}$, the measured $\delta g(\mathbf{r}, E = 30\text{meV}, B)$ shown in Fig. 9B contains distinct modulations within each halo. Fourier analysis yields $|\delta \tilde{g}(\mathbf{q}, 30\text{meV})|$ as shown in Fig. 9C, reveals a set of eight maxima at $\mathbf{q} = [\mathbf{P}_x; \mathbf{P}_y] \approx [(\pm \frac{1}{8}, 0); (0, \pm \frac{1}{8})] 2\pi/a_0$ which we label \mathbf{P} , and at $\mathbf{q} \approx [(\pm \frac{1}{4}, 0); (0, \pm \frac{1}{4})] 2\pi/a_0$ which we label $2\mathbf{P}$. The inset to Fig. 9C shows the measured amplitude $|\delta \tilde{g}(\mathbf{q}, 30\text{meV})|$ along $(1, 0)$ indicating that the field-induced $N(\mathbf{r}, E)$ modulations occur, with both $\lambda \approx 8a_0$ and $\lambda \approx 4a_0$, along both the $(1, 0); (0, 1)$ directions within every vortex halo. The fitted widths $\delta(\mathbf{P})$ of all $|\mathbf{P}| \approx (1/8)2\pi/a_0$ peaks are close to half that of the $|2\mathbf{P}| \approx 1/4(2\pi/a_0)$ peaks: $\delta(2\mathbf{P}) = 1.8 \pm 0.2)\delta(\mathbf{P})$. These phenomena occur in a particle-hole symmetric manner for $25 < |E| < 45 \text{ meV}$ and exhibit predominantly s -symmetry form factor modulations at \mathbf{P} and $2\mathbf{P}$. Finally, measured field-induced energy gap modulations $\delta\Delta(\mathbf{r}) = \Delta(\mathbf{r}, B) - \Delta(\mathbf{r}, 0)$ yield a Fourier transform

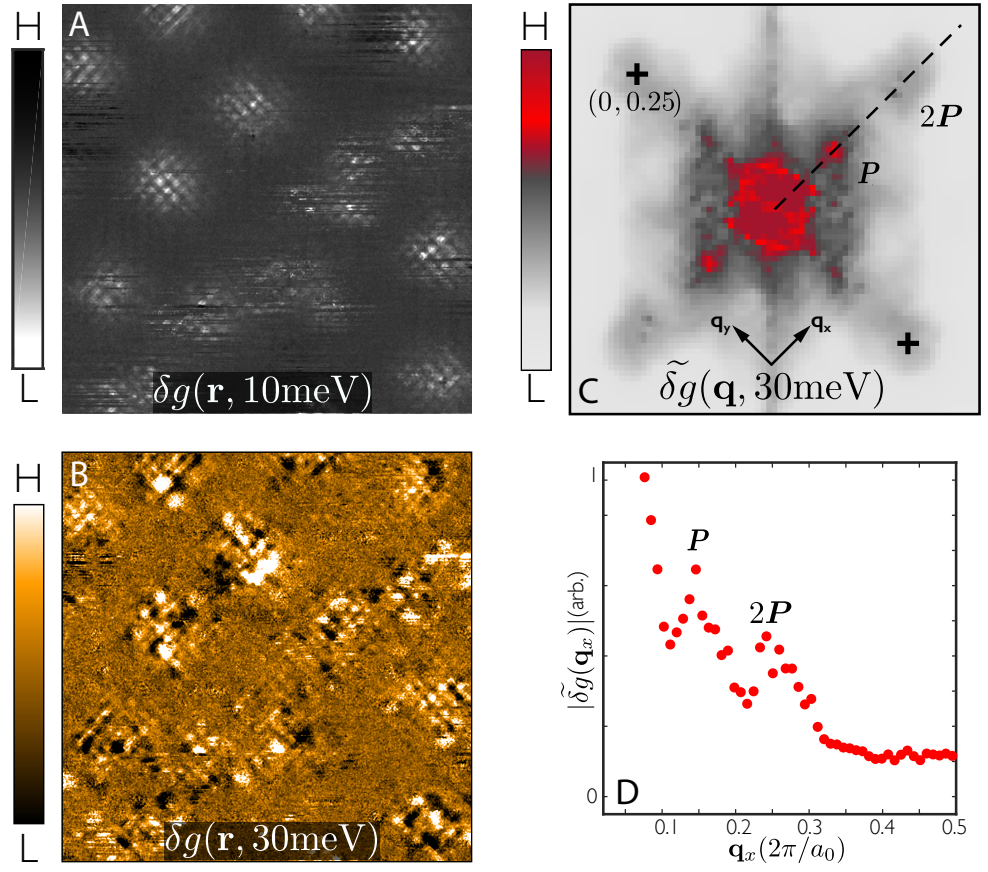


Figure 9

A Measured $\delta g(\mathbf{r}, E, B) = g(\mathbf{r}, E = 10\text{meV}, B = 8.25\text{T}) - g(\mathbf{r}, E = 10\text{meV}, B = 0\text{T})$ in a $58\text{nm} \times 58\text{nm}$ FOV, showing typical examples of the low-energy Bogoliubov quasiparticle modulations within halo regions surrounding four vortex cores in $\text{Bi}_2\text{Sr}_2\text{CaCu}_2\text{O}_{8+\delta}$. **B** Measured field-induced modulations $\delta g(\mathbf{r}, E = 30\text{meV}, B) = g(\mathbf{r}, E = 30\text{meV}, B = 8.25\text{T}) - g(\mathbf{r}, E = 30\text{meV}, B = 0\text{T})$ in the same $58\text{nm} \times 58\text{nm}$ FOV. Although the vortex halos are clearly seen to occur at exactly same locations as in A, the modulations therein are radically different. **C** Amplitude Fourier transform $|\tilde{\delta g}(\mathbf{q}, 30\text{meV})|$ (square root of power spectral density) of $\delta g(\mathbf{r}, E = 30\text{meV}, B)$ data in B. The $\tilde{q} \approx [(\pm\frac{1}{4}, 0); (0, \pm\frac{1}{4})]2\pi/a_0$ points are indicated by black crosses. Four sharp maxima, indicated by P , occur at $\mathbf{q} = [P_x; P_y] \approx [(\pm\frac{1}{8}, 0); (0, \pm\frac{1}{8})]2\pi/a_0$ whereas four broader maxima, indicated by $2P$ occur at $\tilde{q} \approx [(\pm\frac{1}{4}, 0); (0, \pm\frac{1}{4})]2\pi/a_0$. **D** Measured $|\tilde{\delta g}(\mathbf{q}, 30\text{meV})|$ along $(0,0)$ - $(1/2,0)$ showing the two distinct maxima in the field induced $N(\mathbf{r})$ modulations, occurring at by $P = 0.117 \pm 0.01$ and $2P = 0.231 \pm 0.01$. (Data from Edkins *et al.* (15))

$\tilde{\Delta}(\mathbf{q})$ that exhibits energy-gap modulation at P but not at $2P$.

In the context of Ginzburg-Landau theory (12, 13, 14, 15), these data indicate that, in $\text{Bi}_2\text{Sr}_2\text{CaCu}_2\text{O}_{8+\delta}$, a field-induced pair density wave state emerges within the halo region surrounding each quantized vortex core.

3.2.3. Evidence for a PDW in $\text{Bi}_2\text{Sr}_2\text{CaCu}_2\text{O}_{8+\delta}$ at Zero Magnetic Field. Atomic-resolution superconducting STM tips (72) have also been applied for the study of the PDW state in underdoped cuprates, but at $B=0$. Ideally, if both the tip and sample are superconducting, with identical superconducting energy gaps $\Delta(\vec{r})$ and quantum phase difference ϕ , a Josephson current $I(\phi) = I_J \sin(\phi)$ of Cooper pairs can ensue. However, for nanometer scale junctions with normal-state resistance in the GOhm range, thermal fluctuations will overwhelm stable-phase Josephson tunneling until the sub-millikelvin temperature range. Instead, phase-diffusion dominated Josephson tunneling is usually achieved, in which the measured $I(V)$ exhibits a maximum current $I_c \propto I_J^2$ (73). Measuring $I_c(\mathbf{r})$ has therefore become the established approach for visualizing the variation of Josephson tunnelling (73, 74, 75, 76) and thus of superfluid density $\rho_s(\mathbf{r})$.

In a PDW of the type $\Delta_{PDW}^P(\mathbf{r}) = F_{pdw} \Delta_P(\mathbf{r}) [\exp(i\mathbf{P} \cdot \mathbf{r}) + \exp(-i\mathbf{P} \cdot \mathbf{r})]$, the superfluid density $\rho_s(\mathbf{r})$ modulates spatially. Searches for such phenomena in cuprates required visualizing $I_c(\mathbf{r})$ with nanometer resolution, high I_J , low R_N and low operating temperatures. For the $\text{Bi}_2\text{Sr}_2\text{CaCu}_2\text{O}_{8+\delta}$ samples ($T_c = 88\text{K}$, $p =$

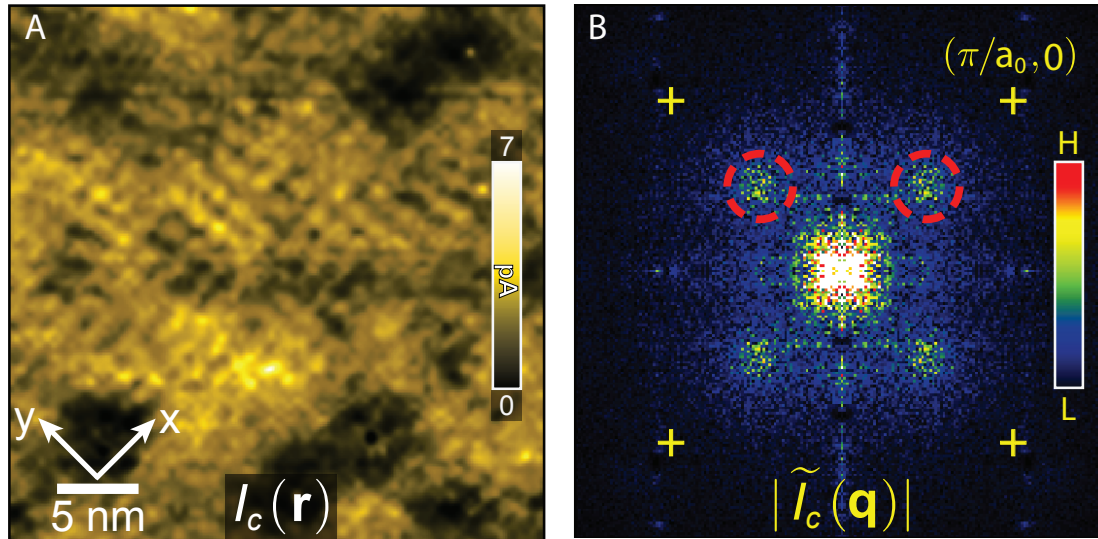


Figure 10

A Typical $I_c(\mathbf{r})$ image from $\text{Bi}_2\text{Sr}_2\text{CaCu}_2\text{O}_{8+\delta}$ at $p = 0.17\%$. The $I_c(\mathbf{r})$ modulations are parallel to the CuO_2 directions (structural supermodulation-induced $I_c(\mathbf{r})$ modulations along the $(1,1)$ directions are removed). **B** $|I_c(\mathbf{q})|$, the Fourier transform of $I_c(\mathbf{r})$ (crosses at $\mathbf{q} = (\pi/a_0, 0); (0, \pi/a_0)$). Maxima from $I_c(\mathbf{r})$ modulations (dashed red circles) occur at $\mathbf{q} = (0.25, 0)2\pi/a_0; (0, 0.25)2\pi/a_0$. (Data from Hamidian *et al.* (77)).

0.17) studied by Hamidian *et al.* (77), the STM operates below 50mK, and high I_J achieved using an exfoliated nanometer-sized flake of $\text{Bi}_2\text{Sr}_2\text{CaCu}_2\text{O}_{8+\delta}$ with spatial resolution $\sim 1\text{nm}$ adhering to the end of each tungsten STM tip. Figure 10A shows a typical $I_c(\mathbf{r})$ image measured under those conditions, clearly exhibiting periodic modulations in $\rho_s(\mathbf{r})$ along the CuO_2 axes $(1,0);(0,1)$. Figure 10B shows $|\tilde{I}_c(\mathbf{q})|$, the magnitude of the Fourier transform of $I_c(\mathbf{r})$, indicating that the wavevectors of $\rho_s(\mathbf{r})$ modulations in $\text{Bi}_2\text{Sr}_2\text{CaCu}_2\text{O}_{8+\delta}$ are at $\mathbf{q} = (0.25 \pm 0.02, 0)2\pi/a_0; (0, 0.25 \pm 0.02)2\pi/a_0$.

Single-electron tunneling SISTM studies on equivalent $\text{Bi}_2\text{Sr}_2\text{CaCu}_2\text{O}_{8+\delta}$ crystals reveal intense electronic structure modulations (78, 79, 80) that are locally commensurate (81, 82), unidirectional (80, 83), exhibit $4a_0$ periodicity (81, 82) with a d -symmetry form factor (83, 84), and are concentrated at particle-hole symmetric energies $|E| \approx \Delta_1$ where Δ_1 is the pseudogap energy scale. (67, 79, 80, 83).

At values of p where simultaneous data exist, the wavelengths of these modulations is indistinguishable from those in $I_c(\mathbf{r})$ within joint uncertainty. While this is consistent with a composite PDW order formed out of a CDW with the same wave-vector and the uniform d -wave superconductivity, whether the order parameter of the fundamental state underpinning these single-electron signatures is a CDW or a PDW remains to be determined. The relationship of the $I_c(\mathbf{r})$ modulations observed at zero magnetic field to the PDW in vortex halos also remains unclear, as it is yet to be established whether the $\lambda \approx 4a_0$ $I_c(\mathbf{r})$ modulations could be consistent with an underlying $\lambda \approx 8a_0$ PDW.

Nevertheless, the $I_c(\mathbf{r})$ imaging data (e.g Fig. 10) provide strong direct evidence for the existence of an PDW coexisting with a robust homogeneous Cooper-pair condensate in underdoped $\text{Bi}_2\text{Sr}_2\text{CaCu}_2\text{O}_{8+\delta}$.

4. OTHER SYSTEMS

4.1. Organics, Fe-based superconductors, and heavy fermion materials

A variety of materials that have been argued to be candidates for the originally proposed FFLO state, in which a Zeeman field shifts the energy of the up-spin and down-spin partners of the Cooper pairs in opposite directions, such that it becomes energetically beneficial to create Cooper pairs with finite momentum. The materials discussed in this section have been reviewed previously (85, 86, 87), so here we highlight the main results and refer to these reviews for more detail.

The most compelling case for realizing the original FFLO-like PDW superconductor (1, 2) is in organic materials. A detailed overview of the experimental evidence for this in quasi-2D organic materials with in-plane magnetic fields is given in Ref. (85). Organic materials have proven to be ideal for realizing the FFLO-like PDW phase for three reasons: they are quasi-2D, suppressing the creation of vortices and allowing the high fields needed to create FFLO-like PDW states to be reached; they are clean with mean free paths typically a

factor of 10-100 greater than the superconducting coherence length; and they have weak spin-orbit coupling. The primary evidence for the existence of the FFLO state is largely of three types: the observation of the characteristic upturn of the upper critical field at low temperatures; the observation of two high-field phase transitions at low temperatures; and the observation of an inhomogeneous magnetic field distribution consistent with that expected for a FFLO-like phase. κ -(BEDT-TTF)₂Cu(NCS)₂ presents the strongest case in which: magnetic torque measurements suggest a first order transition line at high fields inside the superconducting state (88, 89); specific heat measurements observing the same first order transition (90); NMR measurements consistent with the observation of spin-polarized quasiparticles localized near the spatial nodes of the FFLO order parameters (91); and evidence of multiple phase transitions in rf-penetration depth measurements (92). Among the quasi-2D organics there is also evidence for a FFLO-like PDW state in λ -(BETS)₂GaCl₄ (93, 94) and β' -(ET)₂SF₅CH₂CF₂SO₃ (95, 96). In addition, resistivity measurements observe an upper critical field and field anisotropy behavior consistent with a FFLO-like PDW state in the quasi-1d organic (TMTSF)₂ClO₄ (97).

Arguments have been presented that Fe-based superconductors, due to their high upper critical fields, also represent a likely class of materials in which to realize a FFLO-state (98). To date, experimental evidence has been found for a FFLO-like PDW state in KFe₂As₂ (99) where magnetic torque and specific heat measurements observe two superconducting transitions at high fields and observe a characteristic upturn of the upper critical-field at low-temperatures.

Finally, there were reports that FFLO phases also appear in the heavy fermions superconductors UPd₂Al₃ (100, 101), CeRu₂ (101, 102), and CeCoIn₅ (103, 104). However, it has been argued that the phase transition attributed to the FFLO-like PDW phase in both UPd₂Al₃ and CeRu₂ is likely a consequence of a vortex related transition (86). The case for CeCoIn₅ is much more interesting. Subsequent to the original discovery of a new low-temperature, high-field superconducting phase that was argued to be a FFLO-like PDW phase(103, 104), it was found that this phase had spin-density wave (SDW) order (105). This SDW order exists only within the superconducting state. Due to the coexistence of usual superconductivity and SDW order, PDW order will also generically exist (17), making it difficult to identify a primary order parameter. This has led to many proposals that are still being experimentally untangled (87).

4.2. Pair Density Wave in degenerate atomic gases: FFLO

Experimental progress in trapping, cooling and coherently manipulating Feshbach-resonant atomic gases opened unprecedented opportunities to study degenerate strongly interacting quantum many-body systems in a broad range of previously unexplored regimes (106, 107, 108, 109, 110). This has led to a realization of paired fermionic superfluids (111, 112, 113) and the associated Bardeen-Cooper-Schrieffer (BCS) to Bose-Einstein condensation (BEC) crossover (114, 115, 116).

These neutral atomic systems are particularly well-suited to imposing (pseudo-) magnetization, corresponding to the number imbalance $P \equiv (N_{\uparrow} - N_{\downarrow})/N$ in the pairing hyperfine $\uparrow - \downarrow$ species, circumventing challenges of charged electronic superconductors realized in solid state, as discussed in much of this review (117, 118, 119, 120). The imbalance and the associated Fermi surface mismatch frustrate the singlet paired state (121, 122, 123, 124) driving quantum phase transitions out of the gapped BCS superfluid to a variety of putative ground states and thermodynamic phases (125, 126, 127, 128, 129, 130). One of the most interesting is the FFLO finite-momentum paired state (1, 2), that was proposed in mid 60s, but never conclusively observed.

Experiments(117, 118, 119, 120) on trapped atomic systems have extensively explored and established the predicted interaction-imbalance phase diagram, illustrated in Fig.11 (127, 131, 132), dominated by the superfluid to (polarized) Fermi-liquid first-order phase transition, that manifests in phase separation (123, 131, 128). However, outside of one dimension, so far, no signatures of the enigmatic FFLO Pair Density Wave state (1, 2) have been seen. Although naively, this is consistent with the narrowness of the FFLO sliver in the predicted phase diagram (127, 131), much remains to be understood about FFLO's stability, beyond mean-field analyses of simplest FFLO states (133, 134).

In contrast, in one dimension (where it is robust and generic at any nonzero imbalance) the FFLO state has been experimentally realized in a two-dimensional array of decoupled one-dimensional traps, generated via a two-dimensional optical periodic potential(135). Although spin-resolved density profiles in these experiments shows consistency with the FFLO interpretation, they still lack the “smoking gun” observation of e.g., a finite momentum condensate peak in the momentum distribution function, precluded in thermodynamic limit in one dimension by strong quantum and thermal fluctuations and by the inhomogeneous atomic density special to trapped gases.

Experimental efforts are under way to move toward quasi-one-dimensional limit of coupled tubes, and in fact the 1d-3d crossover signatures have been experimentally demonstrated (136, 137). This is done by

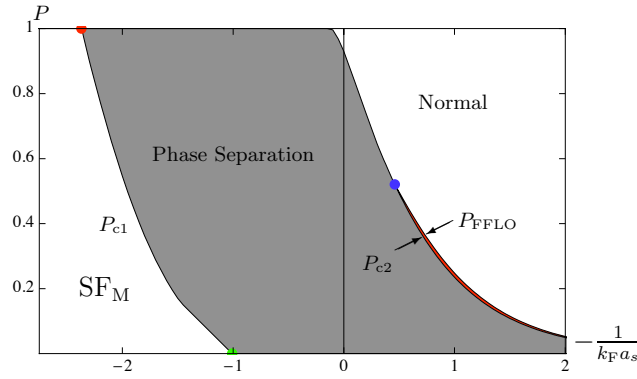


Figure 11

A mean-field zero-temperature phase diagram from Refs.(127, 131) of an imbalanced Fermi gas, as a function of the inverse scattering length and normalized species imbalance (dimensionless magnetization) $P = (N_{\uparrow} - N_{\downarrow})/N \equiv \Delta N/N$, showing the magnetized (imbalanced) superfluid (SF_M), the FFLO state (approximated as the simplest FF state, confined to a narrow red sliver bounded by P_{FFLO} and P_{c2}) and the imbalanced normal Fermi liquid.

reducing the strength of the periodic optical potential, thereby allowing the 1d PDWs of neighboring tubes to lock through inter-tube coupling. Cooling and equilibration, particularly for pseudo-spin remains a challenging experimental problem.

5. MECHANISM

5.1. Evidence of PDW in Models of Strongly Correlated Systems

Condensates with finite momentum are problematic in conventional BCS theory. In the first place, so long as either time-reversal or inversion symmetry is preserved, the Fermi surface is always perfectly nested for some form of $\mathbf{P} = \mathbf{0}$ pairing, *i.e.* the superconducting susceptibility is peaked and logarithmically divergent as $T \rightarrow 0$, while it remains finite at all non-vanishing \mathbf{P} . If the $\mathbf{P} = \mathbf{0}$ divergence is quenched, as it is in any singlet channel by a finite Zeeman field, as recognized Fulde and Ferrell (2) and by Larkin and Ovchinnikov (1) the pair susceptibility can be peaked at a non-zero \mathbf{P} , but in that case it remains finite even as $T \rightarrow 0$. In the Hartree-Fock approximation, used in BCS theory, lack of nesting leads to a finite critical coupling for the condensate to occur even at zero temperature. In the case of FFLO states, the Zeeman coupling to the external magnetic field acts as a small tuning parameter, *i.e.* the critical coupling can still be parametrically small.

In contrast, for the putative PDW states of high T_c superconductors (HTSC) which occur in the absence of an external Zeeman coupling, no such small tuning parameter exists. Even the naive application of BCS theory to PDW states typically requires a critical coupling of strength comparable to the band-width. More importantly, the superconducting states in these materials, uniform or not, arise in strongly correlated systems whose “normal state” is a “strange metal”, a metallic state without well defined fermionic quasiparticles.

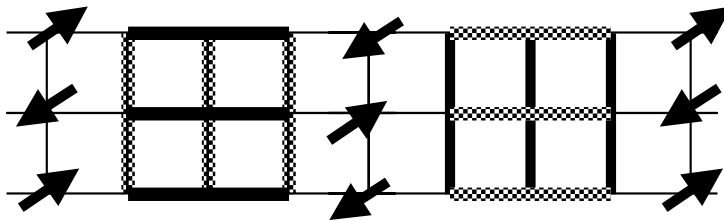


Figure 12

Qualitative picture of the PDW. The local superconducting order parameter is d -wave: positive (negative) in the bold (shaded) links, and axes rotate after a half-period. In this example, presumably applicable to LBCO, the PDW is intertwined with spin stripe order. Notice that the charge density has half the period of the PDW order (from Berg et al. (4)).

The PDW looks locally like a d -wave superconductor. It breaks translation symmetry in such a way that

the order parameter changes sign upon translation by half a period (see Fig.12). Therefore, it is reasonable to suppose that it is a close competitor of the uniform d -wave superconductor under strong-coupling circumstances in which correlation lengths are short and the important physics is correspondingly local. Indeed, in the context of a proposed SO(5) theory of intertwined antiferromagnetic and d -wave superconducting order, it was proposed in 1998 by Zhang (138) some time ago that a “SO(5) spiral” state consisting of alternating stripes of Néel order and d -wave superconducting order – precisely the sort of intertwined PDW and spin stripe shown in Fig.12 – might arise in some circumstances. A variety of subsequent studies employing variational wave functions have also found such states, starting with the 2002 study of Himeda, Kato and Ogata (3) who used variational Monte Carlo calculations of Gutzwiller-projected wave functions for the ground state of the $t - t' - J$ model. These states are inhomogeneous versions of the doped RVB wave functions widely used as candidate ground states for the $t - J$ model. These early results, as well as later variational and renormalized mean field studies (139, 140, 58), found three states whose variational ground state energies are very close: the uniform d -wave superconductor, the PDW state, and a striped d -wave superconductor. For doping near $x = 1/8$, these variational studies found period 4 states with half-filled stripes. The intertwined nature of the PDW states was also proposed on phenomenological grounds in refs. (4, 6, 7).

BCS mean-field methods have also been used to describe PDW phases. Loder and coworkers (141, 53) used BCS mean field theory for a 2D system with a $t-t'$ band structure widely used in the cuprates, and an effective attractive interaction for electrons on nearest-neighboring sites of strength V (assumed to originate from spin fluctuations). Within a BCS type mean field theory these authors find that while in the weak coupling regime the ground state is an uniform d -wave superconductor, for systems near $1/8$ doping, for V larger than a critical value $V_c \gtrsim t$, the preferred pairing state is locally d -wave but has a finite momentum, i.e. a pair-density-wave, with or without an associated spin stripe state. A subsequent publication by Wårdth and Granath found that V_c is significantly larger than this estimate (142). They proposed a model with an interaction with local attraction and longer range phase slip pair hopping and found, using a BCS type theory, that the critical coupling for the PDW state is significantly reduced, and typically of the order of the kinetic energy bandwidth (142, 143).

Other microscopic mechanisms have also been proposed and studied within mean-field approaches. Lee proposed an Amperean pairing mechanism (7), due to local spin current fluctuations in a RVB type state (144), and showed (in mean field theory) that it favors a PDW. Soto-Garrido and Fradkin (145) studied the superconducting condensates arising in the vicinity of a (Pomeranchuk) instability in the quadrupolar spin triplet channel of a Fermi liquid (146), and found that the PDW competes with a spin triplet p and a spin singlet d wave superconducting states. Soto-Garrido and coworkers (147) used a quasi-1D approach based on a model of stripe phases (148) and found PDW states.

At present, the only model that has been definitively shown to have a PDW state is in a model of strongly correlated systems in one dimension known as the Kondo-Heisenberg chain. This model consists of a 1D system of mobile electrons, a Luttinger liquid, coupled by a local Kondo exchange interaction J_K to a spin-1/2 quantum Heisenberg antiferromagnetic chain with exchange coupling J_H . Models of this type have been studied for a long time in the context of the physics of heavy-fermion superconductors. Bosonization and density-matrix renormalization group (DMRG) studies by Sikkema, Affleck and White revealed that for $J_H \gtrsim J_K$ this system has a spin gap (149), which was subsequently interpreted as an exotic η -pairing superconducting state (150, 151). Specifically, the dominant long-range (power-law) correlations involve an oscillatory charge $2e$ order parameter, but it is a composite order in the sense that it cannot be simply expressed as a product of two electron creation operators. Berg, Fradkin and Kivelson (152) reexamined this system by DMRG and showed that it is indeed a PDW state, albeit an exotic one. Specifically, on open chains with different boundary conditions, they showed that in this state all the fermion bilinear operators decay exponentially with distance. Only order parameters that are composite operators of the Luttinger liquid and the spin chain have (quasi) long range order, as suggested by the bosonization studies. For instance, the PDW order parameter is realized as the scalar product of the Néel order parameter of the spin chain with the spin triplet superconductor of the Luttinger liquid, and has quasi-long-range order. (Remarkably, later work showed that this incarnation of the PDW is actually a topological superconductor (153).) Similar behavior was found for the expected charge $4e$ uniform superconducting order parameter. Later on, similar results were found for extended generalized Hubbard models on 2-leg ladders at special filling fractions of the bonding band (154).

A real challenge is to establish the existence of a PDW state in two dimensions using unbiased approaches, even numerically. Due to the notorious fermion sign problem, quantum Monte Carlo type methods are only useful at relatively high temperatures, and have not been able to reach low enough temperatures to see unambiguous signs of d -wave superconductivity in Hubbard models and its generalizations. None-the-less, down to the lowest temperatures accessible, such calculations always find a superconducting susceptibility that is peaked at $\mathbf{P} = \mathbf{0}$ (155). On the other hand exact diagonalizations can only deal with systems which are too small to be useful to detect PDW states (even if they were ground states). One option is DMRG simulations

on relatively wide ladders, and we will discuss these shortly. DMRG methods are known to be asymptotically exact matrix-product states (at least for gapped states), whose accuracy can be improved by increasing the bond dimension of the tensors. These approaches are known to generate large enough quantum entanglement to produce most states of interest in one-dimensional systems, including quantum critical states.

Another option are tensor network approaches which, conceptually, are extensions of DMRG to higher dimensions. However, while in 1D it is known that matrix product states are sufficient to describe most systems of interest, in higher dimensions this is an open question. The current most widely used tensor network approach is PEPS (projected entangled paired states) (156). PEPS, and its relative iPEPS (infinite PEPS), consist of a variational ansatz in the form of a tensor network (a matrix product state) with a large number of variational parameters that grow as a power of the “bond dimension” (the dimension of the tensor), of order $3D^4$ where D is the bond dimension. Unlike conventional variational wavefunctions, which are essentially product states (and hence have only short-range entanglement), iPEPS can describe more complex states with large-scale entanglement. Corboz and coworkers (157) initiated a study of the $t - J$ model as a function of doping. In the most recent study of this type (158) it was found that, for a wide range of parameters J/t and doping δ the uniform d -wave superconductor, the striped superconductor, and the PDW (called the “anti-phase” stripe state by Corboz et al), are essentially degenerate. Although this result agrees with the simpler variational wave functions discussed above, in the iPEPS generated states the charge stripes are not half-filled and, in fact, their occupancy varies continuously with J/t . (Were such a PDW state to be relevant in the cuprates, its period would not be particularly pinned to $8a$, even near $1/8$ doping, in contrast with experiment in LBCO.) The iPEPS results are highly encouraging for the existence of PDW order. However, we should be careful to note that it is unclear at the present time what biases are implied in this approach, and these results need to be “benchmarked” against other techniques.

Quite recently, large-scale DMRG simulations of the $t - J$ model on 4-leg ladders in the doping range $5\% - 12.5\%$ with $t/J = 3$ (and other values as well) (159, 160, 161) have been carried out. These authors find strong evidence for d -wave superconductivity (i.e. a sign change of the superconducting amplitude along two orthogonal directions) and charge-stripe phases with $1/2$ a hole per unit cell. These simulations kept a significantly larger number of states in the DMRG than earlier studies. However, although the parameter range examined by these authors is broad and overlaps with those used in the iPEPS simulations discussed above, no evidence for PDW states have (yet) been detected in the DMRG. This result is in apparent contradiction with the iPEPS results, and this discrepancy is quite puzzling. This is a pressing problem a deeper understanding of the advantages and limitations of these methods is clearly required. A recent DMRG study of a doped $t - J$ model on a triangular lattice with ring exchange interactions found encouraging evidence of PDW-like superconducting correlations that change sign as a function of distance, but which fall sufficiently rapidly (at least like r^{-4}) that they do not give rise to a diverging susceptibility as $T \rightarrow 0$. (162).

We close this section by noting that PDW states have been studied using methods of holography, the AdS-CFT correspondence. Although it is not clear what microscopic systems can be described with holography, these theories have the clear advantage of describing metallic states without well defined quasiparticles (163). Several holographic models have been published describing superconductors with striped phases (164), and systems with intertwined superconducting and PDW orders (165, 166, 167).

5.2. Fulde-Ferrell-Larkin-Ovchinnikov state in degenerate atomic gases

One context in which a FFLO state has a well-understood microscopic mechanism is a singlet superconductor with pairing frustrated by a magnetic field (168, 169, 170, 2, 1). An ideal realization of such a system is a pseudo-spin imbalanced Feshbach-resonant atomic Fermi gas (117, 118, 119, 120), where (in contrast to charged electronic superconductors in solid state), the Zeeman component of the magnetic field and the effective magnetization can be tuned *independently* of the obscuring orbital field effects, such as vortices. This has rekindled extensive theoretical research (121, 122, 123, 124, 171, 127, 131, 128, 130, 132, 137), reviewed in Refs. (110, 10).

5.2.1. Model of a resonant Fermi gas. A neutral fermionic atomic gas is well captured by a microscopic Hamiltonian

$$H = \sum_{\mathbf{k}, \sigma} (\epsilon_{\mathbf{k}} - \mu_{\sigma}) \hat{c}_{\mathbf{k}\sigma}^{\dagger} \hat{c}_{\mathbf{k}\sigma} + g \sum_{\mathbf{k}\mathbf{k}'\mathbf{q}} \hat{c}_{\mathbf{k}\uparrow}^{\dagger} \hat{c}_{-\mathbf{k}+\mathbf{q}\downarrow}^{\dagger} \hat{c}_{-\mathbf{k}'+\mathbf{q}\downarrow} \hat{c}_{\mathbf{k}'\uparrow}. \quad 8.$$

with the single-particle energy $\epsilon_{\mathbf{k}} = \hbar^2 k^2 / 2m$. The separately conserved number $N_{\sigma} = (N_{\uparrow}, N_{\downarrow})$ of atomic species (hyperfine states) $\sigma = (\uparrow, \downarrow)$ are imposed by two chemical potentials, $\mu_{\sigma} = (\mu_{\uparrow}, \mu_{\downarrow})$ or equivalently by the average chemical potential $\mu = \frac{1}{2}(\mu_{\uparrow} + \mu_{\downarrow})$ and the Zeeman field $h = \frac{1}{2}(\mu_{\uparrow} - \mu_{\downarrow})$, that respectively tune the total atom number $N = N_{\uparrow} + N_{\downarrow}$ and atom pseudo-spin imbalance $\Delta N = N_{\uparrow} - N_{\downarrow}$.

Key features that distinguishes this Fermi system from those familiar electronic ones in solid state contexts (discussed in other parts of this review) are (i) the fermions are neutral and thus do not couple to the electromagnetic vector potential, (ii) absence of a periodic ionic potential (though an optical lattice can be imposed by an off-resonant interfering laser fields) that explicitly breaks rotational and translational spatial symmetries, (iii) the *resonant* nature of the Feshbach interaction, parameterized by a short-range s-wave pseudopotential, $g < 0$. The resulting attractive interaction can be computed through an exact T -matrix scattering analysis (108), with g controlling the magnetic-field tunable (172) 3D scattering length

$$a_s(g) = \frac{m}{4\pi} \frac{g}{1 + g/g_c}, \quad 9a.$$

that diverges above a critical attraction strength, $|g| = g_c \equiv 2\pi^2 d/m$, corresponding to a threshold for a two-atom bound state of size d .

The Zeeman h field-driven Fermi surface mismatch (that, for these *neutral* fermions can be tuned independently of the orbital field, and can also be realized via atomic mass and other dispersion imbalance), energetically penalizing the conventional BCS $-\mathbf{k}$ to \mathbf{k} pairing at weak coupling. However, as was first predicted by Fulde and Ferrell(2), and Larkin and Ovchinnikov(1), a finite momentum \mathbf{P} pairing, $\Delta_{\mathbf{P}} = \sum_{\mathbf{k}} g \langle c_{-\mathbf{k}\downarrow} c_{\mathbf{k}+\mathbf{P}\uparrow} \rangle$, (set by the Fermi surface mismatch) allows for FFLO ground state, that compromises between a fully paired superconductor and a magnetized Fermi liquid.

The simplest treatment is a mean-field analysis(127, 131) for the PDW order parameter $\Delta(\mathbf{r}) = \sum_{\mathbf{p}} \Delta_{\mathbf{p}} e^{i\mathbf{p}\cdot\mathbf{r}} = g \langle \hat{c}_{\downarrow}(\mathbf{r}) \hat{c}_{\uparrow}(\mathbf{r}) \rangle$, generalized to pair-condensation at a set of reciprocal lattice vectors, \mathbf{p} , with the amplitudes $\Delta_{\mathbf{p}}$ and \mathbf{p} self-consistently determined by the minimizing the ground state energy. This gives a satisfactory qualitative description (quantitatively valid deep in the weakly-coupled BCS regime, $k_F |a_s| \ll 1$), as a starting point of more sophisticated large- N_f (173, 174) and ϵ -expansions (175) treatments.

5.2.2. Ginzburg-Landau model and transitions to FFLO state. Starting at a high Zeeman field, above the Chandrasekhar-Clogston-Pauli limit (168, 169), $h_c = \Delta_{BCS}/\sqrt{2}$ (a critical field for a direct first-order mean-field transition from a Fermi-liquid (FL) to a uniform BCS superconductor), inside the polarized Fermi liquid and reducing h , one finds (in mean-field) a continuous transition at $h_{c2} \approx \frac{3}{4} \Delta_{BCS} > h_c$ to a FFLO superconductor(1, 2, 127, 131) (stable for $h_{c1} < h < h_{c2}$), most strongly paired at a momentum with magnitude $p_0 \approx 1.2h_{c2}/v_F \approx 1.81\Delta_{BCS}/v_F$. This is captured by a Ginzburg-Landau expansion (derived by integrating out the fermions (134)) for the ground-state energy density,

$$\mathcal{H} \approx \sum_{\mathbf{p}} \varepsilon_{\mathbf{p}} |\Delta_{\mathbf{p}}|^2 + \sum_{\{\mathbf{p}_i\}} V_{\mathbf{p}_1, \mathbf{p}_2, \mathbf{p}_3, \mathbf{p}_4} \Delta_{\mathbf{p}_1}^* \Delta_{\mathbf{p}_2} \Delta_{\mathbf{p}_3}^* \Delta_{\mathbf{p}_4}, \quad 10.$$

valid for a weak finite-momentum pairing amplitude Δ_p near the continuous Fermi-liquid (FL) to FFLO phase transition at h_{c2} . It is notable that this expansion is analytic at small Δ_p , in contrast to a vanishing Zeeman field, that at zero temperature exhibits $|\Delta|^2 \ln \Delta$ nonanalyticity. The finite momentum instability is captured by the dispersion (127, 131, 134)

$$\begin{aligned} \varepsilon_p &\approx \frac{3n}{4\epsilon_F} \left[-1 + \frac{1}{2} \ln \frac{v_F^2 p^2 - 4h^2}{\Delta_{BCS}^2} + \frac{h}{v_F p} \ln \frac{v_F p + 2h}{v_F p - 2h} \right], \\ &\approx J(p^2 - p_0^2)^2 + \varepsilon_{p_0}, \end{aligned} \quad 11.$$

whose minimum at a finite $p_0(h) \approx 1.2h/v_F$ (near h_{c2}) captures the polarized Fermi system's energetic tendency to pair at a finite momentum, forming a FFLO state at a fundamental reciprocal lattice vector with a magnitude p_0 . The Zeeman energy h_{c2} at which $\varepsilon_{p_0}(h)$ vanishes determines the corresponding mean-field FL-FFLO phase transition point.

As in other problems of periodic ordering (e.g., crystallization), in the absence of an underlying lattice (as in trapped atomic gases) ε_p is rotationally invariant, and thus, the quadratic $|\Delta_{\mathbf{p}}|^2$ term only selects the fundamental *magnitude* of the reciprocal lattice, $|\mathbf{p}| = p_0$, with all orientations degenerate, becoming unstable simultaneously at h_{c2} . This contrasts qualitatively with PDW ordering in solid state, where the underlying ionic crystal explicitly breaks rotational and translational symmetries, selecting a discrete set of \mathbf{p} momenta, as discussed in Sec. 2. In the rotationally and translationally invariant trapped atomic gases, it is the quartic and higher order nonlinearities in $\Delta_{\mathbf{p}}$ that select the structure of the FFLO state, characterized by reciprocal lattice of \mathbf{p} 's and the corresponding amplitudes, $\Delta_{\mathbf{p}}$. Near h_{c2} it is the $(-\mathbf{p}, \mathbf{p})$ LO state (1) with $\Delta_{LO}(\mathbf{r}) = \Delta_{L0} \cos \mathbf{p} \cdot \mathbf{r}$, that is energetically preferred over the single plane-wave FF state, $\Delta_{FF}(\mathbf{r}) = \Delta_{FF} e^{i\mathbf{p}\cdot\mathbf{r}}$ (1, 2). However, no study has conclusively determined the structure of the FFLO state throughout the field-interaction ($h - 1/k_F a$) phase diagram, despite heroic efforts in the relativistic QCD context (176, 177).

Near h_{c2} , the *unidirectional* pair-density wave (Cooper-pair stripe) order, characterized by a *collinear* set of \mathbf{p}_n 's is well captured by focusing on long-wavelength fluctuations of these most unstable modes. The state

is well described by a Ginzburg-Landau Hamiltonian density

$$\mathcal{H} = J [|\nabla^2 \Delta|^2 - 2p_0^2 |\nabla \Delta|^2] + r |\Delta|^2 + \frac{1}{2} \lambda_1 |\Delta|^4 + \frac{1}{2} \lambda_2 \mathbf{j}^2, \quad 12.$$

where deep in the BCS limit, near h_{c2} the model parameters are given by

$$J \approx \frac{0.61n}{\epsilon_F p_0^4}, \quad p_0 \approx \frac{1.81 \Delta_{BCS}}{\hbar v_F}, \quad r \approx \frac{3n}{4\epsilon_F} \ln \left[\frac{9h}{4h_{c2}} \right], \quad 13a.$$

$$h_{c2} \approx \frac{3}{4} \Delta_{BCS}, \quad \lambda_1 \approx \frac{3n}{4\epsilon_F \Delta_{BCS}^2}, \quad \lambda_2 \approx \frac{1.83nm^2}{\epsilon_F \Delta_{BCS}^2 p_0^2}, \quad 13b.$$

and the inclusion of the current-current interaction, $\mathbf{j} = \frac{1}{m} \text{Re}[-\Delta^*(\mathbf{r})i\nabla\Delta(\mathbf{r})]$ is necessary for a complete description of the transverse superfluid stiffness.

Well below h_{c2} , the PDW order parameter $\Delta_{\mathbf{p}}$ is no longer small, invalidating the above Ginzburg-Landau expansion and requiring a complementary weak h Bogoliubov-deGennes (BdG) treatment, that is fully non-linear in $\Delta(\mathbf{r})$. However, it is challenging to handle analytically for anything other than a single harmonic FF state, $\Delta_{FF}(\mathbf{r}) = \Delta_{FF} e^{i\mathbf{p}\cdot\mathbf{r}}$, as it requires a fully self-consistent BdG band-structure analysis, with energetics strongly dependent on the details of the FFLO state. A single-harmonic BdG calculation(127, 131) finds that a BCS singlet superconductor is unstable to the FF state at $h_{c1} \approx 0.70\Delta_{BCS}$, thus suggesting that PDW state is stable only over a very narrow range of h .

However, numerical BdG analyses (178, 179, 180) and a negative domain-wall energy in an otherwise fully-paired singlet BCS superfluid in a Zeeman field(180, 181) argue that a more generic pair-density wave state (that includes a larger set of collinear wavevectors) may be significantly more stable. Well below h_{c2} the FFLO state is thus more accurately described as a periodic array of solitons, well-paired $\pm\Delta_{BCS}$ stripes interrupted by “normal” gapless domain-walls that accommodate the imposed fermion imbalance, driven by h . This state can be equivalently thought of as a periodically ordered *micro*-phase separation between the normal and paired states, that naturally replaces the *macro*-phase separation(182, 123) ubiquitously found in the BCS-BEC detuning-imbalance phase diagram (127, 183, 131, 132) (see Fig.11). Upon increasing h above h_{c1} the excess of the majority fermionic atoms (polarization) in an imbalanced system can be *continuously* accommodated by the sub-gap states localized on the self-consistently induced domain-walls between $+\Delta$ and $-\Delta$. Thus the imbalance and density of domain-walls continuously grows above h_{c1} eventually overlapping at h_{c2} and thereby interpolating between the two limiting forms of the LO state. This picture resembles the soliton mechanism for doping of polyacetylene (184), and is explicitly realized in one-dimension (1d) through exact BdG (178) and Bethe ansatz (185, 186) solutions and via bosonization(187, 188), that exhibits the commensurate-incommensurate (CI) Pokrovsky-Talapov (PT) transition (189) from a fully paired s-wave superfluid to a Larkin-Ovchinnikov state. Such phenomenology also emerges from the numerical BdG studies in two dimensions(179, 180). This response to a Zeeman field is quite analogous to the more familiar phenomenology of type-II superconductor in an orbital magnetic field, with fully-gapped BCS, partially paired FFLO and fully depaired normal FL playing the role of the Meissner, Abrikosov vortex lattice and normal states, respectively.

5.2.3. Goldstone modes and topological excitations. Trapped atomic gases (in the absence of an optical lattice) exhibit underlying translational and rotational symmetries. Thus, as we discuss below, in addition to the off-diagonal-long-range order, the FFLO states break *continuous* spatial symmetries, and hence exhibit unusual Goldstone modes and novel topological defects. This contrasts qualitatively with the putative solid state PDW realizations (formulated in Sec. 2 and discussed in the rest of the review), where spatial symmetries are broken *explicitly* by the underlying crystal, and, thus, orientational Goldstone modes are absent.

Inspired by the one dimensional picture discussed above, a class of striped unidirectional FFLO, with Cooper pairs condensed at a co-linear set of wavevectors $\mathbf{p}_n = n\mathbf{p}_0$, has received considerable attention. The FF plane wave and LO standing wave states are qualitatively accurate representatives, that have been extensively explored (110, 10). In particular, beyond mean-field theory, the time-reversal breaking FF state is characterized by an order parameter $\Delta_{FF}(\mathbf{r}) = \Delta_{p_0} e^{i\mathbf{p}_0\cdot\mathbf{r} + i\phi(\mathbf{r})}$, with a single Goldstone mode $\phi(\mathbf{r})$, that in addition to superfluid phase fluctuations, also describes local fluctuations in the orientation of FF stripes. Because in a trapped atomic gas context, free of the underlying lattice, FF state spontaneously breaks rotational (but not translational) symmetry, the energetics of $\phi(\mathbf{r})$ is qualitatively “softer”, with the Hamiltonian (derivable from the microscopics, above GL theory, or deduced based on symmetry)

$$\mathcal{H}_{FF} = \frac{1}{2} \chi^{-1} n^2 + \frac{1}{2} K (\nabla^2 \phi)^2 + \frac{1}{2} \rho_s^{\parallel} (\partial_{\parallel} \phi)^2, \quad 14.$$

where $\partial_{\parallel} \equiv \hat{\mathbf{p}}_0 \cdot \nabla$, $\rho_s^{\parallel} = 8Jp^2 |\Delta_{p_0}|^2$ is the superfluid stiffness along p_0 , $K = 2J |\Delta_{p_0}|$, and n the density operator (only well-defined on a lattice), canonically conjugate to the phase field ϕ . The spontaneous breaking of rotational symmetry requires a strict vanishing of FF’s transverse superfluid stiffness, $\rho_s^{\perp} = 0$.(190, 133, 134)

The time-reversal preserving LO state spontaneously breaks both rotational and translational symmetries, with a $(-\mathbf{p}_0, \mathbf{p}_0)$ order parameter

$$\Delta_{LO}(\mathbf{r}) = 2\Delta_{p_0} e^{i\phi} \cos[\mathbf{p}_0 \cdot \mathbf{r} + \theta], \quad 15a.$$

that is a *product* of a superfluid and a unidirectional density wave order parameters. These are respectively characterized by two Goldstone modes $\phi(\mathbf{r}), \theta(\mathbf{r})$, corresponding to the superfluid phase and the smectic phonon $u(\mathbf{r}) = -\theta(\mathbf{r})/p_0$ of the striped state.

Similarly to the FF state, the underlying rotational symmetry of the LO state strongly restricts the form of the Goldstone-mode Hamiltonian. Namely, its $\theta(\mathbf{r}) = -p_0 u(\mathbf{r})$ sector must be invariant under a rotation of \mathbf{p}_0 , that defines the spontaneously-chosen orientation of the pair-density wave, and therefore must be described by a smectic form (191, 192, 193). On the other hand because a rotation of the LO state leaves the superconducting phase, $\phi(\mathbf{r})$ unchanged, the superfluid phase $\phi(\mathbf{r})$ sector of the Hamiltonian is therefore expected to be of a conventional xy -model type. Consistent with these symmetry-based expectations the LO Goldstone-mode Hamiltonian was indeed found(133, 134) to be given by

$$\begin{aligned} \mathcal{H}_{LO} = & \frac{1}{2}\Pi^2 + \frac{1}{2}K(\nabla^2 u)^2 + \frac{1}{2}B(\partial_{\parallel} u)^2 \\ & + \frac{1}{2}\chi^{-1}n^2 + \frac{1}{2}\rho_s^{\parallel}(\partial_{\parallel}\phi)^2 + \frac{1}{2}\rho_s^{\perp}(\nabla_{\perp}\phi)^2, \end{aligned} \quad 16.$$

with Π the momentum operator field, canonically conjugate to the phonon u . Thus, the LO state is a highly anisotropic superfluid (though less so than the FF state, where $\rho_s^{\perp} = 0$), with

$$\frac{\rho_s^{\perp}}{\rho_s^{\parallel}} = \frac{3}{4} \left(\frac{\Delta_{p_0}}{\Delta_{BCS}} \right)^2 \approx \frac{1}{4} \ln \left(\frac{hc_2}{h} \right) \ll 1, \quad 17.$$

a ratio that vanishes for $h \rightarrow h_{c_2}^-$.(133, 134)

We note that in the presence of underlying rotational invariance, at nonzero temperature, the collinear FFLO states exhibit a 3d quasi-long-range translational order. Thus, the translational symmetry is restored and somewhat oxymoronically, the FFLO order parameter $\Delta_{\mathbf{P}}$ vanishes inside a collinear FFLO phase. Consequently, the uniform Δ_{4e} is the fundamental nonzero order parameter at any nonzero temperature.

In addition to Goldstone modes, the low-energy phenomenology is also controlled by topological defects, that in conventional superfluids are limited to 2π vortices in the superfluid phase $\phi(\mathbf{r})$. In stark contrast, the additional LO phonon Goldstone mode $\theta(\mathbf{r})$ also admits 2π vortices, corresponding to an integer a dislocation in the striped LO order. Even more interestingly, as also discussed in Section 2.1, in addition to these integer vortex $(\pm 2\pi, 0)$ and dislocation $(0, \pm 2\pi)$ defects, the product nature of the LO order parameter, (15) allows for half-integer vortex-dislocation composite defects, $(\pm\pi, \pm\pi)$.(5, 133, 11, 134, 7) The sequential unbinding of this larger class of defects leads to a rich variety of LO descendent phases. Many interesting consequences such as three-dimensional quasi-long-range order, importance of Goldstone-mode nonlinearities, charge $4e$ superconductivity, exotic topological phases and transitions of the enriched nature of the FF and LO states have been extensively explored in Refs.(133, 134, 110).

Finally, we note that although the bosonic sector of the FFLO state, discussed above is well understood, the problem is seriously complicated by the gapless fermions confined to the $\pm\Delta$ domain-walls of the PDW. These will certainly lead to damping of the bosonic Goldstone modes. Coupling between the gapless fermions confined to strongly fluctuating FFLO phonons remain a challenging open problem, some aspects of which are discussed in Ref.(134).

5.3. Nonuniform pairing in non-centrosymmetric and Weyl superconductors

Nonuniform pairing states with FFLO-like pairing mechanism have also been obtained in non-centrosymmetric systems (194, 195). In general these systems involve pairing on Fermi surfaces whose centers do not sit at high symmetry points in the Brillouin zone, and thus the Cooper pairs forming from these Fermi surfaces carry nonzero momentum.

One such scenario is for a metal with Rashba spin-orbit coupling in an in-plane Zeeman field H :

$$H = \frac{\mathbf{k}^2}{2m} - \mu + \lambda(\mathbf{k} \times \boldsymbol{\sigma}) \cdot \hat{z} - \mu_B H \sigma_x \quad 18.$$

The superconducting instabilities of the concentric split FS's at $H = 0$ have been analyzed in Ref. (196) (see also Ref. (197)). With $H \neq 0$, in the limit $\mu_B H \ll \lambda k_F$, the two split FS's approximately retain their shapes and get relatively shifted by $\pm \mathbf{P}/2$, where $\mathbf{P} = \frac{2\mu_B H}{v_F} \hat{\mathbf{y}}$, shown in Fig. 13. Naturally, the finite-momentum pairing order parameters that couples as $\Delta_{\pm \mathbf{P}} c^{\dagger}(\mathbf{k} \pm \mathbf{P}/2) c^{\dagger}(-\mathbf{k} \pm \mathbf{P}/2)$, which separately gap out the two

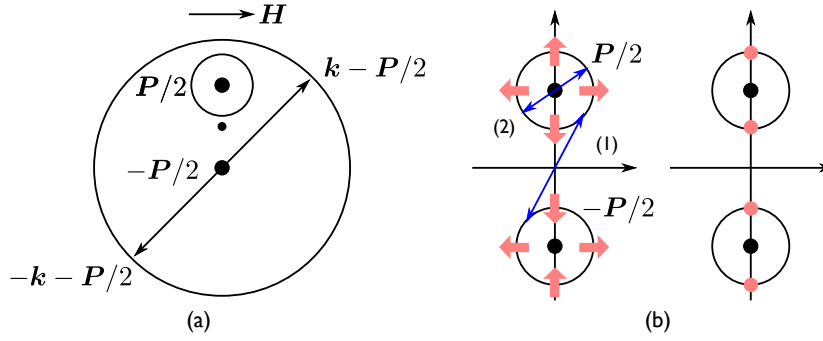


Figure 13

Panel(a): The split Fermi surfaces described by Eq. 18. Figure adapted from Ref. (194). Panel (b): Left: spin texture on the Weyl FS's, and various Cooper pairs. Arrows (1,2) shows Cooper pairs in a uniform SC state, but for (2) the fermions have the same spin, and a singlet pairing gap vanishes here. Arrow (3) shows the Cooper pairs in a PDW state with intra-FS pairing. Right: The point nodes in the spin-singlet pairing state. A more generic reasoning for point nodes was given later; see main text. Figure adapted from Ref. (198).

shifted split FS's. Compared with the FFLO scenario in which only a small part of the FS is gapped, the present state has a larger condensation energy and can potentially be realized at relatively small coupling.

Three pairing states have been theoretically investigated in Refs. (199, 194, 195): a uniform pairing order, an FF-like “helical” pairing order with only one ordering momentum (say Δ_{+P}), and an LO-like stripe pairing order with both $\Delta_{\pm P}$. Note that unlike a canonical PDW state where Δ_P and Δ_{-P} are related by inversion and time-reversal symmetry, here both symmetries are explicitly broken already in the normal state. In this case, symmetry arguments on the Ginzburg-Landau free energy imply the superconducting ground state generally has finite-momentum pairing (200). In more microscopic studies, it was indeed obtained that the finite-momentum pairing orders including helical order and stripe order occupy sizable regions in the pairing phase diagram as a function of temperature and the in-plane Zeeman field (194, 195). Properties of these nonuniform pairing states in non-centrosymmetric materials have been reviewed in Ref. (201)

Signatures of such a stripe PDW-like state were indeed observed in proximitized HgTe Quantum Wells (202). When gated to electron-doped regime, HgTe quantum well exhibits split FS's with Rashba spin-orbit coupling. The quantum well is coupled to a conventional superconductor on one side and subject to an in-plane magnetic field \mathbf{B} . As \mathbf{B} varies, the oscillation of the Josephson current across the quantum well has been observed, which is evidence for finite-momentum pairing order induced in HgTe. The in-plane Zeeman field either can be an external field, or can be realized intrinsically. In Ref. (203) PDW pairing has been proposed for SrTiO₃-LaAlO₃ oxide interfaces, which exhibits coexistence between ferromagnetism and superconducting orders. It was shown that the RKKY interaction between the local moments drive the interface into a ferromagnetic phase. Together with the Rashba spin-orbit coupling, the system was proposed to realize a PDW-like state via the aforementioned mechanism. Another context of this mechanism for nonuniform pairing is the surface superconductivity on topological insulators (TI). Much of the attention towards TI-surface superconductivity has been focused on its realization of topological superconductivity, i.e., the well-known Fu-Kane superconductivity (204). On the other hand, with a nonzero chemical potential, it is straightforward to see that the surfaces also hosts $\pm P/2$ -shifted Fermi surfaces with a spin texture (205). However, unlike the FS in Fig. 13, the two FS's are located at opposite spatial surfaces. Moreover, inversion symmetry is not necessarily broken in the three-dimensional system, thus the two Fermi surfaces can have the same size. Remarkably, there is recently experimental evidence observing finite- P pairing on topological insulators surfaces with an in-plane Zeeman field. (206)

An interesting extension of this mechanism for the nonuniform pairing state is to 3d systems with Fermi surfaces not centered around any high symmetry points $\pm P/2$ (198, 207, 208, 209). The simplest way of obtaining these FS's is from doping a Weyl semimetal, which does not require any symmetry to stabilize. A simple two-band lattice model given by Ref. (198) describing this situation is

$$H_0 = t(\sigma^x \sin k_x + \sigma^y \sin k_y) + t_z(\cos k_z - \cos(P/2))\sigma^z + m(2 - \cos k_x - \cos k_y)\sigma^z - \mu \quad 19.$$

For small chemical potential μ , each spherical FS encloses a Weyl point at $\pm P/2$ and is spin-textured, analogous to the 2d case with Rashba spin-orbit coupling (see Fig 13(a) for a $k_y = 0$ slice).

Both intra-FS and inter-FS pairing can potentially occur, giving rise to a PDW-like state with ordering momenta $\pm P$ and a uniform SC state respectively. The energetic interplay between PDW and uniform SC depends on several factors. First, unlike the previous case where the FS's remain symmetric about their shifted

centers for small H , here in general there are no symmetry relating $\epsilon(\mathbf{k} + \mathbf{P}/2) = \epsilon(-\mathbf{k} - \mathbf{P}/2)$ unless μ is very small. Either way, the susceptibility towards a PDW state is reduced, while typically inversion symmetry (for the present case with two Weyl nodes) or time-reversal symmetry (e.g., for cases with four Weyl nodes) guarantees a weak-coupling instability towards a uniform SC. On the other hand, there is a robust topological reason that the uniform SC order parameter has point nodes, which tends to suppress the uniform SC. This was first observed in Ref. (198) and formulated in generic cases in Ref. (208). Weyl points are monopoles of the Berry curvature $\vec{\mathcal{B}}(\mathbf{k}) = i\langle \nabla_{\mathbf{k}} u(\mathbf{k}) | \times | \nabla_{\mathbf{k}} u(\mathbf{k}) \rangle$ in \mathbf{k} space. Weyl points at $\pm \mathbf{P}/2$ carry monopole charges ± 1 , and this monopole charge is equal to the Berry flux through its enclosing FS. In the Nambu space of the pairing Hamiltonian, the Berry fluxes through the electron-like FS and hole-like shadow FS subject to pairing, or the monopole charges adds up. It was shown that (208, 209) the total monopole charge inside the original FS is 2 for uniform (inter-FS) SC, and is 0 for (intra-FS) PDW. This means that the uniform SC state has to host at least two point nodes on each Fermi surface, independent of any microscopic details. The PDW state can be fully gapped, likely leading to a higher condensation energy.

The detailed interplay between these two opposite effects has been examined in Ref. (207) with short-range attractive interactions in PDW and SC channels, and the authors found that PDW state is favored for a noncentrosymmetric Weyl metal. However, in more realistic systems a more careful examination on the band structure and the interaction is needed to pin down the superconducting ground state.

6. BROADER RELEVANCE

In the preceding sections we presented evidence of the existence of pair-density-wave superconducting order in diverse systems ranging from cuprate high temperature superconductors to heavy fermionic materials to organics to topological materials, as well in cold atomic systems. Unlike its FFLO predecessors, the PDW discussed in the context of the Cuprate family does not require an external magnetic field for its existence.

As reviewed in earlier sections, the PDW is a new state of matter with unique properties not encountered in other superconductors. It is a superconducting state with more than one complex order parameter. Its more complicated order parameter manifold allows this state to accommodate various charge orders, together with superconducting states, some even with an exotic flux quantization. This richness leads, in a natural way, to an explanation of several intriguing experimental effects, such as dynamical layer decoupling and a rich structure of superconducting vortices. These features also imply a complex phase diagram with a variety of broken symmetry phases.

Given the evidence that PDW order appears in some places in the cuprate phase diagram, it remains to discuss the implication of this observation in the broader context of cuprate physics (and beyond). Up to now the evidence comes primarily from two groups of experiments on two groups of materials. First, as reviewed in section 3.1, the layer decoupling observed in 1/8 doped LBCO led to the suggestion that PDW order with substantial range correlations exists over a sizeable temperature range before the onset of 3D uniform d-wave pairing. This suggestion has been leant further credibility by the observation of a variety of other related phenomena, such as the detection of an anomalously large second harmonic in the Josephson relation in LBCO-Nb junctions and the appearance of the familiar signatures of layer decoupling in other 214 materials when stripe order is enhanced, including LSCO in a magnetic field. Second, a CDW with wave-vector equal to half of what is commonly observed was seen in the vicinity of the vortex core in underdoped Bi-2212 (15). As such a CDW subharmonic is expected as a consequence of coexisting uniform and PDW order, its observation provides strong evidence of the existence of PDW in the vortex halo, as discussed in section 3.2.

It is worth mentioning that none of these pieces of evidence is entirely immune to the possibility of alternative explanations; indeed, in all cases there are additional experimental observations that while not actually contradictory with the PDW interpretation, are also not entirely natural. Most importantly, to date no diffraction experiments have detected the expected CDW subharmonic associated with the coexistence of PDW and uniform SC correlations, either in LBCO or in the magnetic field and temperature regimes that have been so far explored in YBCO and BSCCO. Conversely, in the range of T in which layer decoupling gives strong evidence of dominantly PDW correlations in 1/8 doped LBCO, ARPES data have been interpreted (210) (see fig 1) as showing a nodal-d-wave-like one electron spectrum, rather than the nodal-arc spectrum expected for a pure PDW. In all cases, there are multiple possible ways one can imagine reconciling these observations with the PDW interpretation. However, ultimately we will rely on further experiments (some of which are discussed below) to resolve these issues.

Putting these concerns aside, a key question is whether these PDW “sightings” are relevant only in the relatively narrow context of cuprates with certain structural peculiarities (such as LBCO) or in the vicinity of isolated vortex cores, or whether they have broader implications to the physics of underdoped cuprates. In particular, the question arises whether PDW correlations are in any way responsible for the so-called “pseudo-gap regime” observed in underdoped cuprates. For the purpose of this review, we will focus the discussion of

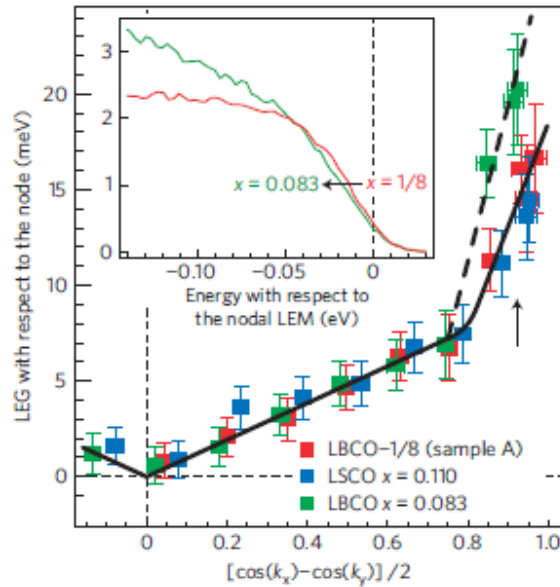


Figure 14

LBCO and LSCO gap, from He et al. (210)

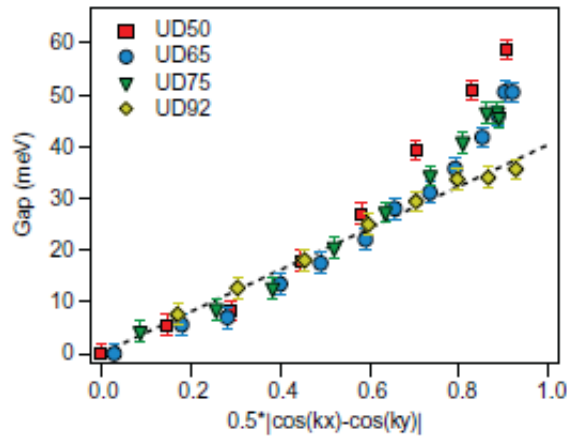


Figure 15

Bi-2212 gap, from Lee et al. (211)

this question on the range of hole doping from $p \sim 0.08$ to 0.15 in which there is an identifiable temperature scale, T^* , below which various measurable properties show a depletion of the density of states at low energies. This thus pertains to an intermediate doping range between very low doping where physics is dominated by significant local antiferromagnetic order and the high doping region where a full Fermi surface enclosing $1 + p$ holes forms. Note that T^* is at largest 300K-400K, which is still low compared with microscopic scales such as the exchange scale J . A phenomenon closely associated with this T^* scale is the appearance of a deep depression in the single-particle spectral weight (*i.e.* the eponymous pseudo-gap) in the anti-nodal portion of the Fermi surface up to T^* , which in turn can be much higher than T_c . This pseudo-gap has been seen in not only in ARPES data and but also by STM, as shown in Fig. 16; importantly, since STM accesses both the unoccupied and occupied states, it reveals an approximate particle-hole symmetry of this gap. This suggests that the gap is associated with some form of SC pairing. On the other hand, certain features of the gap as inferred from ARPES evolve differently as a function of doping and temperature in the near nodal region where the gap is small and in the antinodal region where it is large – the so-called nodal-antinodal dichotomy. This can be seen to some extent in the data from Bi2212 shown in Fig. 15, and more dramatically in the case of LBCO (Fig. 14) and Bi-2201 where detailed ARPES data are available (26). This apparent dichotomy has led many researchers to conclude that the pseudo-gap has a distinct (non-superconducting) origin.

In addition to the energy gap, another striking feature of the underdoped cuprate phase diagram is the

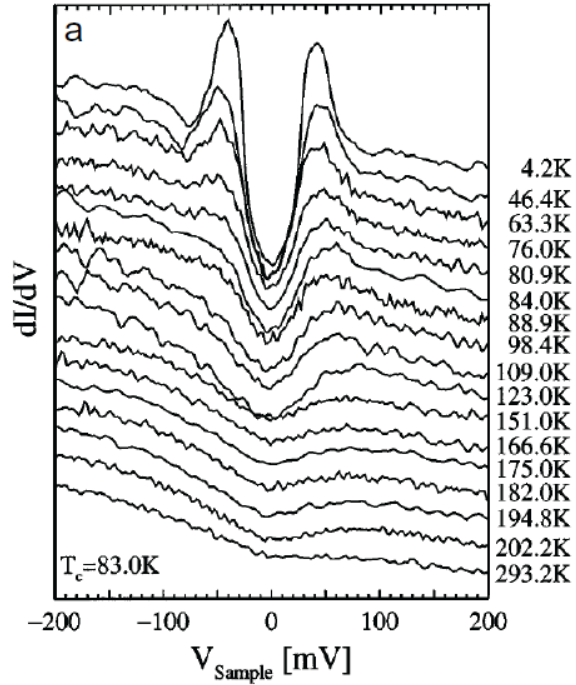


Figure 16

STM pseudogap from Renner et al. (212)

existence of “intertwined” order parameters corresponding to multiple distinct broken symmetry states that occur with similar energy and temperature scales, and which in some ways compete and in some ways cooperate strongly with each other. In addition to the insulating Néel order and uniform d-wave superconducting order, this list includes a variety of other metallic or superconducting spin-density wave, CDW, and nematic orders. To this list we now add PDW order. It seems unreasonable that these materials should be accidentally fine-tuned close to an extraordinarily complex multicritical point at which all these orders are degenerate with each other, so it is reasonable to search for a description in which the observed orders derive from a smaller set of “primary” order parameters.

The underlying idea is that, under certain circumstances, some class of “soft” fluctuations can partially melt a parent broken symmetry state in such a way that some but not all the underlying symmetries are restored, leaving behind a partially ordered state with some form of vestigial order (213). Formally, as discussed in Sec. 2, this corresponds to forming composite order parameters that are bilinear (or higher order) in the primary order parameter fields. In the present context, starting from an assumed primary PDW order parameter, one can readily construct composite orders corresponding to both CDW order and nematic orders making it possible to view these as vestigial orders remaining when a fully ordered PDW is partially melted by strong phase fluctuations.

There are several phenomenologically appealing aspects of this perspective. With regards to nematic order, while there is suggestive evidence that it arises at temperature scales comparable to the pseudo-gap T^* , it is very difficult to see how a primary nematic order could be responsible for the pseudo-gap, but viewed as a composite order, it can be understood as an avatar of a more basic set of correlations. Similarly, the observed CDW order is mostly weak in the sense that it causes unusually small magnitude lattice distortions, which is why it was overlooked for so many years. (LBCO may be an exception.) The CDW does not open gaps or fold the Fermi surface observed in ARPES in ways that are familiar from other classes of CDW materials. (26) Still, CDW order appears to be thermodynamically robust in both the sense that significant CDW correlations persist over a wide range of T and p , and that it appears to compete on a more or less equal footing with the uniform d-wave SC state, for instance in that there is a clear suppression of the superconducting T_c in the range of dopings where the CDW correlations are strongest, while high T_c can be restored with the application of modest pressure, presumably because this suppresses the CDW tendency. Again, viewing the CDW as a composite order gives a rationale for viewing it as being simultaneously weak and strong in different aspects.

At a more local level, there has long been strong intuitive appeal to viewing the pseudo-gap as a form of local pairing without any significant SC phase coherence. The fact that the pseudo-gap shares so many obvious similarities with the d-wave SC gap is, of course, the strongest piece of evidence in favor of this

interpretation. For instance, at low temperatures, the gap seen in ARPES in Bi-2212 for a range of doping roughly in the range $0.12 < p < 0.19$, the gap magnitude along the Fermi surface has the simplest d-wave form, $\Delta_0[(\cos(k_x) - \cos(k_y))/2]$. This gap is presumably well understood as being due to the d-wave SC state. However, there is a distinct difference in the thermal evolution of the near nodal and antinodal gaps - an aspect of the previously mentioned nodal anti-nodal dichotomy. In particular, in the anti-nodal regime of the BZ, the gap magnitude is only very weakly T dependent and it evolves smoothly into the pseudo-gap that persists to well above T_c . Moreover, as seen in Fig. 15 as a function of decreasing p , the energy gap below T_c at the antinode starts to grow strongly but continuously, i.e. the gap structure increasingly looks like the sum of a near nodal superconducting gap (whose magnitude is in fact largely independent of p down to $p \approx 0.07$) plus another gap which is large at the antinode and small or vanishing in an arc region near the nodal point. In the context of the present work, it is tempting to associate this evolution with an increasingly significant admixture of a PDW component in the gap structure. Also, at least in one material where detailed ARPES spectra is available, Bi-2201, the top of the gap does not line up with the location of the Fermi momentum, as one would expect for a uniform superconductor, but is consistent with a momentum carrying condensate, such as the PDW (26, 7). While it may be possible to account for the differences in the thermal evolution of the gap in the nodal and antinodal regimes as a purely kinematic effect of phase fluctuations in a simple d-wave superconductor (214, 215), the nodal anti-nodal dichotomy has been taken as evidence against fluctuating d-wave as the origin of the pseudo-gap at the anti-node (216, 217). The PDW seems like a natural candidate that is next in line.

To summarize, there remains the larger question of the broader significance of the PDW in the phase diagram of the cuprates and, particularly, of its role in the pseudogap regime. We find it useful to focus on two extremal perspectives which lie at the opposite ends of a spectrum of possibilities. For ease of discussion, we will label the first view as “competing order” and the second view as “mother state.”

In the “competing order” perspective, the PDW is a close competitor of uniform d-wave superconductivity and of the observed CDW orders, which are to be regarded as independent (although strongly coupled) order parameters. Their interplay may change from one family of cuprates to another (or in a particular family as a function of doping) depending on other factors, e.g. the crystal structure, whether SDW order plays a role or not, etc. This is especially clear in the case of LBCO, where the critical temperatures are comparable, which naturally leads to the notion that they may have a common microscopic origin (and, in this sense, are intertwined). Nevertheless, this does not necessarily imply that they should not be regarded as completely separate orders. This is because there are terms in the Landau theory of the type presented in earlier sections, e.g. trilinear couplings of the form $\rho_{2P}\Delta_{\mathbf{P}}^*\Delta_{-\mathbf{P}}$. Physically, these terms can be interpreted as saying that there should be a non-vanishing value of the CDW order ρ_{2P} as soon as the PDW order parameter is present, $|\Delta_{\pm\mathbf{P}}| \neq 0$, i.e. $\rho_{\mathbf{P}} \propto \Delta_{-\mathbf{P}}^*\Delta_{\mathbf{P}}$, and the CDW order is a composite order. However, this coupling can also be interpreted as saying that as ρ_{2P} becomes sufficiently strong, the quadratic term of the PDW order can acquire a negative coefficient which when large enough, can induce a PDW order parameter $\Delta_{\pm\mathbf{P}}$.

A convenient mathematical language to describe competing order is the nonlinear σ model. This has been employed to describe the appearance of static PDW in the vicinity of the vortex core, where d-wave order smoothly rotates to a PDW order (13). Another situation for its application may be the onset of layer decoupling driven by a magnetic field in LSCO (46). In that case one may envision a rotation to a PDW from a d-wave under the influence of magnetic field driven spin order.

A second perspective is to regard the PDW as the primary order (the “mother state”), and to regard other orders (e.g. CDW) as composite (or descendant) orders. If the low temperature phase is indeed a PDW, then the other orders may appear through a partial melting cascade of phase transitions. In these regimes, the CDW (and nematic) orders are vestigial orders of the PDW, and the PDW itself can be regarded as a “fluctuating” order.

As a fluctuating order, the PDW is locally defined on some length scale without ever being the ground state. The correlation length should be long enough to form the antinodal gap and to induce the composite orders, but short enough that the properties usually associated with superfluidity are not apparent. Taken to its logical conclusion, this point of view states that PDW fluctuations is pervasive over a large part of the doping, temperature and magnetic field range of the phase diagram and is the root cause of the pseudogap phenomenology. This view has been strongly advocated by one of us (7), while a more guarded proposal that fluctuating PDW may be responsible for the pseudo-gap structure at the anti-node and the Fermi arc near the node have been made earlier (6). The appeal of this picture is that it reduces the explanation of the panoply of observed orders to the existence of local PDW orders. Near the vortex core it is suggested that the rapid winding of d-wave vortex can pin the PDW, rendering it static and generate the short range $\mathbf{P}/2$ CDW observed experimentally (218). Just as in the competing order scenario, the PDW provides a mechanism for lowering the vortex core energies and, hence, making H_{c2} parametrically smaller (13). What happens for field greater than H_{c2} is probably the most intriguing open question. One has to face the question of how to describe

a pairing state that has been destroyed by quantum phase fluctuations, which remains an unsolved problem (219). The quantum disordering of a PDW which already breaks translational symmetry and is gapless even in the absence of a magnetic field, is still more clearly terra incognita. Experimentally CDW with longer range order appears with increasing magnetic field and a metallic state with small Fermi pocket emerges. Whether this state can be the result of a fluctuating PDW remains to be seen (220, 7, 27, 6, 221, 222). It is worth noting that the competing order scenario faces the same issue: in the σ model description, an ordered PDW appears when the vortex halo's overlap and one needs to address the question of how this order is destroyed.

Another important question for the “mother state” scenario is whether a coherence length large enough to create an energy gap will necessarily produce large observable consequences of superconducting fluctuations. Experimentally diamagnetic fluctuations have been observed up to two or three times T_c and also above H_{c2} at low temperatures (223, 224). On the other hand there is little transport signatures. Can these observations be reconciled? The ultimate question is whether these ideas and the contrast between the two extreme perspectives can be either directly supported or falsified. In this sense the recent proposal of a method to directly measure PDW fluctuations in a tunnel junction using Bi-2201 as one electrode and take advantage of the known momentum that is present in this material offers some hope for the future (225). Another urgent avenue of research is of course to see whether the \mathbf{P} CDW observed so far by STM can be confirmed by diffraction and whether they exist more generally in other cuprate families.

DISCLOSURE STATEMENT

The authors are not aware of any affiliations, memberships, funding, or financial holdings that might be perceived as affecting the objectivity of this review.

ACKNOWLEDGMENTS

J.C.S.D. acknowledges support from Science Foundation Ireland under Award SFI 17/RP/5445 and from the European Research Council (ERC) under Award DLV-788932. J.C.S.D and S.D.E acknowledge support, and the funding to carry out STM/SJTM studies of cuprate PDWs, from the Gordon and Betty Moore Foundations EPiQS Initiative through Grant GBMF4544. SDE acknowledges support from the Karel Urbanek Postdoctoral Fellowship at Stanford University. SAK was supported in part by NSF grant DMR-1608055. EF was supported in part by NSF grant DMR-1725401. This work was funded by the Office of Basic Energy Sciences, Materials Sciences and Engineering- ing Division, U.S. Department of Energy (DOE) under contracts DE-SC0012368(DVH,EF). DVH was supported in part by NSF grant DMR-1710437. PAL acknowledges support by DOE grant DE-FG02-03ER46076. YW was supported by the Gordon and Betty Moore Foundation EPiQS Initiative through the grant GBMF 4305. LR was supported by the Simons Investigator Award from The James Simons Foundation. JMT was supported at Brookhaven by DOE Contract No. DE-SC0012704. This research was supported in part by the National Science Foundation under Grant No. NSF PHY-1748958 at KITP.

LITERATURE CITED

1. Larkin AI, Ovchinnikov YN. 1964. *Zh. Eksp. Teor. Fiz.* 47:1136. [Sov. Phys. JETP **20**, 762 (1965)]
2. Fulde P, Ferrell RA. 1964. *Phys. Rev.* 135:A550
3. Himeda A, Kato T, Ogata M. 2002. *Phys. Rev. Lett.* 88:117001
4. Berg E, Fradkin E, Kim EA, Kivelson SA, Oganesyan V, et al. 2007. *Phys. Rev. Lett.* 99:127003
5. Agterberg DF, Tsunetsugu H. 2008. *Nature Phys.* 4:639
6. Berg E, Fradkin E, Kivelson SA, Tranquada JM. 2009. *New J. Phys.* 11:115004
7. Lee PA. 2014. *Phys. Rev. X* 4:031017
8. Li Q, Hücker M, Gu GD, Tselik AM, Tranquada JM. 2007. *Phys. Rev. Lett.* 99:067001
9. Casalbuoni R, Nardulli G. 2004. *Rev. Mod. Phys.* 76:263
10. Kinnunen JJ, Baarsma JE, Martikainen JP, Törmä P. 2018. *Reports on Progress in Physics* 81:046401
11. Berg E, Fradkin E, Kivelson SA. 2009. *Nat. Phys.* 5:830–33
12. Agterberg DF, Garaud J. 2015. *Phys. Rev. B* 91:104512
13. Wang Y, Edkins SD, Hamidian MH, Davis JCS, Fradkin E, Kivelson SA. 2018. *Phys. Rev. B* 97:174510
14. Dai Z, Zhang YH, Senthil T, Lee PA. 2018. *Phys. Rev. B* 97:174511
15. Edkins SD, Kostin A, Fujita K, Mackenzie AP, Eisaki H, et al. 2018. Magnetic-Field Induced Pair Density Wave in the Cuprate Vortex Halo. arXiv:1802.04673
16. Fradkin E, Kivelson SA, Tranquada JM. 2015. *Rev. Mod. Phys.* 87:457–482
17. Agterberg DF, Sigrist M, Tsunetsugu H. 2009. *Phys. Rev. Lett.* 102:207004
18. Radzihovsky L, Vishwanath A. 2009. *Phys. Rev. Lett.* 103:010404
19. Radzihovsky L. 2011. *Physical Review A* 84

20. Barci DG, Fradkin E. 2011. *Phys. Rev. B* 83:100509
21. Mross DF, Senthil T. 2015. *Phys. Rev. X* 5:031008
22. Berezinskii V. 1972. *Sov. Phys. JETP* 34:610
23. Kosterlitz J, Thouless D. 1973. *J. Phys. C* 6:1181
24. Jose J, Kadanoff L, Kirkpatrick S, Nelson D. 1977. *Phys. Rev. B* 16:1217
25. Chan C. 2016. *Phys. Rev. B* 93:184514
26. He R, Hashimoto M, Karapetyan H, Koralek J, Hinton J, et al. 2011. *Science* 331:1579
27. Baruch S, Orgad D. 2008. *Phys. Rev. B* 77:174502
28. Harrison N, Sebastian S. 2011. *Phys. Rev. Lett.* 106:226402
29. Wang Y, Agterberg DF, Chubukov A. 2015. *Phys. Rev. Lett.* 114:197001
30. Tu WL, Lee TK. 2019. *Scientific Reports* 9:1719
31. Moodenbaugh AR, Xu Y, Suenaga M, Folkerts TJ, Shelton RN. 1988. *Phys. Rev. B* 38:4596–4600
32. Fujita M, Goka H, Yamada K, Tranquada JM, Regnault LP. 2004. *Phys. Rev. B* 70:104517
33. Hücker M, v. Zimmermann M, Gu GD, Xu ZJ, Wen JS, et al. 2011. *Phys. Rev. B* 83:104506
34. Axe JD, Moudden AH, Hohlwein D, Cox DE, Mohanty KM, et al. 1989. *Phys. Rev. Lett.* 62:2751
35. Axe JD, Crawford MK. 1994. *J. Low Temp. Phys.* 95:271
36. Tranquada JM, Gu GD, Hücker M, Jie Q, Kang HJ, et al. 2008. *Phys. Rev. B* 78:174529
37. Li Q, Hücker M, Gu GD, Tselik AM, Tranquada JM. 2007. *Phys. Rev. Lett.* 99:067001
38. Tranquada JM, Sternlieb BJ, Axe JD, Nakamura Y, Uchida S. 1995. *Nature* 375:561
39. Tajima S, Noda T, Eisaki H, Uchida S. 2001. *Phys. Rev. Lett.* 86:500–503
40. Basov DN, Timusk T. 2005. *Rev. Mod. Phys.* 77:721–779
41. Croft TP, Lester C, Senn MS, Bombardi A, Hayden SM. 2014. *Phys. Rev. B* 89:224513
42. Thampy V, Dean MPM, Christensen NB, Steinke L, Islam Z, et al. 2014. *Phys. Rev. B* 90:100510
43. Suzuki T, Goto T, Chiba K, Shinoda T, Fukase T, et al. 1998. *Phys. Rev. B* 57:R3229–R3232
44. Kimura H, Matsushita H, Hirota K, Endoh Y, Yamada K, et al. 2000. *Phys. Rev. B* 61:14366–14369
45. Lake B, Rønnow HM, Christensen NB, Aeppli G, Lefmann K, et al. 2002. *Nature* 415:299–301
46. Schafgans AA, LaForge AD, Dordevic SV, Qazilbash MM, Padilla WJ, et al. 2010. *Phys. Rev. Lett.* 104:157002
47. Wen J, Jie Q, Li Q, Hücker M, v. Zimmermann M, et al. 2012. *Phys. Rev. B* 85:134513
48. Stegen Z, Han SJ, Wu J, Pramanik AK, Hücker M, et al. 2013. *Phys. Rev. B* 87:064509
49. Zhong R, Schneeloch JA, Chi H, Li Q, Gu G, Tranquada JM. 2018. *Phys. Rev. B* 97:134520
50. He RH, Tanaka K, Mo SK, Sasagawa T, Fujita M, et al. 2009. *Nat. Phys.* 5:119–123
51. Valla T, Federov AV, Lee J, Davis JC, Gu GD. 2006. *Science* 314:1914
52. Razzoli E, Drachuck G, Keren A, Radovic M, Plumb NC, et al. 2013. *Phys. Rev. Lett.* 110:047004
53. Loder F, Graser S, Schmid M, Kampf AP, Kopp T. 2011. *Phys. Rev. Lett.* 107:187001
54. Homes CC, Hücker M, Li Q, Xu ZJ, Wen JS, et al. 2012. *Phys. Rev. B* 85:134510
55. Li Y, Terzic J, Baity PG, Popović D, Gu GD, et al. 2018. Tuning from failed superconductor to failed insulator with magnetic field. arXiv:1810.10646
56. Rajasekaran S, Okamoto J, Mathey L, Fechner M, Thampy V, et al. 2018. *Science* 359:575–579
57. Yuli O, Asulin I, Millo O, Koren G. 2007. *Physical Review B* 75:184521
58. Yang KY, Chen WQ, Rice TM, Sigrist M, Zhang FC. 2009. *New Journal of Physics* 11:055053
59. Yuli O, Asulin I, Koren G, Millo O. 2010. *Physical Review B* 81:024516
60. Yang K. 2013. *J. Supercond. Nov. Magn.* 26:2741–2742
61. Shi Z, Baity PG, Terzic J, Sasagawa T, Popović D. 2019. Destruction of superconductivity by the magnetic field in copper oxides with intertwined charge and spin orders. preprint
62. Buzdin A, Koshelev AE. 2003. *Physical Review B* 67:220504
63. Moshe M, Mints RG. 2007. *Physical Review B* 76:054518
64. Stoutimore MJA, Rossolenko AN, Bolginov VV, Oboznov VA, Rusanov AY, et al. 2018. *Phys. Rev. Lett.* 121:177702
65. Schneider CW, Hammerl G, Logvenov G, Kopp T, Kirtley JR, et al. 2004. *EPL (Europhysics Letters)* 68:86
66. Hamilton DR, Gu GD, Fradkin E, Van Harlingen DJ. 2018. Signatures of pair-density wave order in phase-sensitive measurements of $\text{La}_{2-x}\text{Ba}_x\text{CuO}_{4-\delta}\text{-Nb}$ Josephson junctions and SQUIDS. arXiv:1811.02048
67. Fujita K, Hamidian M, Firmo I, Mukhopadhyay S, Kim CK, et al. 2015. Spectroscopic Imaging STM: Atomic-Scale Visualization of Electronic Structure and Symmetry in Underdoped Cuprates, vol. 180 of *Springer Series in Solid-State Sciences*, chap. 3. Berlin, Heidelberg: Springer Berlin Heidelberg, 73–109
68. Hoffman JE, Hudson EW, Lang KM, Madhavan V, Eisaki H, et al. 2002. *Science* 295:466
69. Matsuba K, Yoshizawa S, Mochizuki Y, Mochiku T, Hirata K, Nishida N. 2007. *Journal of the Physical Society of Japan* 76:063704
70. Yoshizawa S, Koseki T, Matsuba K, Mochiku T, Hirata K, Nishida N. 2013. *Journal of the Physical Society of Japan* 82:083706
71. Machida T, Kohsaka Y, Matsuoaka K, Iwaya K, Hanaguri T, Tamegai T. 2016. *Nature Communications* 7:1–6
72. Pan SH, Hudson EW, Davis JC. 1998. *Applied Physics Letters* 73:2992–2994
73. Naaman O, Teizer W, Dynes RC. 2001. *Phys. Rev. Lett.* 87:097004
74. Rodrigo, J. G., Suderow, H., Vieira, S. 2004. *Eur. Phys. J. B* 40:483–488
75. Proslir, Th., Kohen, A., Noat, Y., Cren, T., Roditchev, D., Sacks, W. 2006. *Europhys. Lett.* 73:962–968
76. Randeria MT, Feldman BE, Drozdov IK, Yazdani A. 2016. *Phys. Rev. B* 93:161115

77. Hamidian M, Edkins S, Joo SH, Kostin A, Eisaki H, et al. 2016. *Nature* 532:343–347
78. Hanaguri T, Lupien C, Kohsaka Y, Lee DH, Azuma M, et al. 2004. *Nature* 430:1001
79. McElroy K, Lee DH, Hoffman JE, Lang KM, Lee J, et al. 2005. *Phys. Rev. Lett.* 94:197005
80. Kohsaka Y, Taylor C, Fujita K, Schmidt A, Lupien C, et al. 2007. *Science* 315:1380–1385
81. Mesaros A, Fujita K, Edkins SD, Hamidian MH, Eisaki H, et al. 2016. *Proceedings of the National Academy of Sciences* 113:12661–12666
82. Zhang Y, Mesaros A, Fujita K, Edkins SD, Hamidian MH, et al. 2018. Using Machine Learning for Scientific Discovery in Electronic Quantum Matter Visualization Experiments. arXiv:1808.00479
83. Hamidian MH, Edkins SD, Kim CK, Davis JC, Mackenzie AP, et al. 2015. *Nature Physics* 12:150
84. Fujita K, Hamidian MH, Edkins SD, Kim CK, Kohsaka Y, et al. 2014. *Proceedings of the National Academy of Sciences* 111:E3026–E3032
85. Agosta C. 2018. *Crystals* 8:285
86. Matsuda Y, Shimahara H. 2007. *J. Phys. Soc. Jpn.* 76:051005
87. Kenzelmann M. 2017. *Rep. Prog. Phys.* 80:034501
88. Bergk B, Demuer A, Sheikin I, Wang Y, Wosnitza J, et al. 2011. *Phys. Rev. B* 83:064506
89. Tsuchiya S, Yamada JI, Sugii K, Graf D, Brooks J, et al. 2015. *J. Phys. Soc. Jpn.* 84:034703
90. Agosta C, Fortune N, Hannahs S, Gu S, Liang L, et al. 2017. *Phys. Rev. Lett.* 118:267001
91. Mayaffre H, Kramer S, Horvatic M, Berthier C, Miyagawa K, et al. 2014. *Nature Physics* 10:928
92. Agosta C, Jin J, Coniglio WA, Smith BE, Cho K, et al. 2012. *Phys. Rev. B* 85:214514
93. Tanatar M, Ishiguro T, Tanaka H, Kobayashi H. 2002. *Phys. Rev. B* 66:134503
94. Coniglio W, Winter L, Cho K, Agosta C, Fravel B, Montgomery LK. 2011. *Phys. Rev. B* 83:224507
95. Koutroulakis G, Kuhne H, Schlueter J, Wosnitza J, Brown S. 2016. *Phys. Rev. Lett.* 116:067003
96. Cho K, Smith BE, Coniglio WA, Winter LE, Agosta CC, Schlueter JA. 2009. *Phys. Rev. B* 79:220507(R)
97. Yonezawa S, Kusaba S, Maeno Y, Auban-Senzier P, Pasquier C, Jerome D. 2008. *Phys. Rev. Lett.* 100:117002
98. Gurevich A. 2010. *Phys. Rev. B* 82:184504
99. Cho CW, Yang J, Yuan N, Shen J, Wolf T, Lortz R. 2017. *Phys. Rev. Lett.* 119:217002
100. Gloos K, Modler R, Schimanski H, Bredl CD, Geibel C, et al. 1993. *Phys. Rev. Lett.* 70:501
101. Modler R, Gegenwart P, Lang M, Deppe M, Weiden M, et al. 1996. *Phys. Rev. Lett.* 76:1292
102. Yamashita A, Ishii K, Yokoo T, Akimitsu J, Hedo M, et al. 1997. *Phys. Rev. Lett.* 79:3771
103. Radovan HA, Fortune NA, Murphy TP, Hannahs ST, Palm EC, et al. 2003. *Nature* 425:51
104. Bianchi A, Movshovich R, Capan C, Pagliuso PG, Sarrao JL. 2003. *Phys. Rev. Lett.* 91:187004
105. Kenzelmann M, Strassle T, Niedermayer C, Sigrist M, Padmanabhan B, et al. 2008. *Science* 321:1652
106. Bloch I, Dalibard J, Zwirger W. 2008. *Rev. Mod. Phys.* 80:885–964
107. Ketterle W, Zwierlein M. 2008. *Rivista del Nuovo Cimento* 164
108. Gurarie V, Radzihovsky L. 2007. *Annals of Physics* 322:2 – 119. January Special Issue 2007
109. Giorgini S, Pitaevskii LP, Stringari S. 2008. *Rev. Mod. Phys.* 80:1215–1274
110. Radzihovsky L, Sheehy D. 2010. *Reports on Progress in Physics* 73:076501
111. Regal CA, Greiner M, Jin DS. 2004. *Phys. Rev. Lett.* 92:040403
112. Zwierlein MW, Stan CA, Schunck CH, Raupach SMF, Kerman AJ, Ketterle W. 2004. *Phys. Rev. Lett.* 92:120403
113. Kinast J, Hemmer SL, Gehm ME, Turlapov A, Thomas JE. 2004. *Phys. Rev. Lett.* 92:150402
114. Eagles DM. 1969. *Phys. Rev.* 186:456–463
115. Leggett A. 1980. Diatomic molecules and Cooper pairs. In *Modern Trends in the Theory of Condensed Matter*, eds. A Pekalski, J Przystawa, vol. 115 of *Lecture Notes in Physics*. Proceedings of the XVI Karpacz Winter School of Theoretical Physics, February 19 – March 3, 1979 Karpacz, Poland, Berlin, Heidelberg: Springer Berlin Heidelberg
116. Nozieres P, Schmitt-Rink S. 1985. *Journal of Low Temperature Physics* 59:195–211
117. Zwierlein MW, Schirotzek A, Schunck CH, Ketterle W. 2006. *Science* 311:492–496
118. Partridge GB, Li W, Kamar RI, Liao Ya, Hulet RG. 2006. *Science* 314:54–54
119. Shin Y, Zwierlein MW, Schunck CH, Schirotzek A, Ketterle W. 2006. *Phys. Rev. Lett.* 97:030401
120. Nascimbène S, Navon N, Chevy F, Salomon C. 2010. *New Journal of Physics* 12:103026
121. Combescot R. 2001. *Europhysics Letters (EPL)* 55:150–156
122. Liu WV, Wilczek F. 2003. *Phys. Rev. Lett.* 90:047002
123. Bedaque PF, Caldas H, Rupak G. 2003. *Phys. Rev. Lett.* 91:247002
124. Caldas H. 2004. *Phys. Rev. A* 69:063602
125. Castorina P, Grasso M, Oertel M, Urban M, Zappalà D. 2005. *Phys. Rev. A* 72:025601
126. Sedrakian A, Mur-Petit J, Polls A, Muther H. 2005. *Physical Review A* 72
127. Sheehy DE, Radzihovsky L. 2006. *Phys. Rev. Lett.* 96:060401
128. Pao CH, Wu ST, Yip SK. 2006. *Phys. Rev. B* 73:132506
129. Son DT, Stephanov MA. 2006. *Phys. Rev. A* 74:013614
130. Bulgac A, Forbes MM, Schwenk A. 2006. *Phys. Rev. Lett.* 97:020402
131. Sheehy DE, Radzihovsky L. 2007. *Annals of Physics* 322:1790 – 1924
132. Parish MM, Marchetti FM, Lamacraft A, Simons BD. 2007. *Nature Physics* 3:124 EP
133. Radzihovsky L, Vishwanath A. 2009. *Phys. Rev. Lett.* 103:010404
134. Radzihovsky L. 2011. *Phys. Rev. A* 84:023611
135. Liao Ya, Rittner ASC, Paprotta T, Li W, Partridge GB, et al. 2010. *Nature* 467:567 EP –

136. Revelle MC, Fry JA, Olsen BA, Hulet RG. 2016. *Phys. Rev. Lett.* 117:235301
137. Parish MM, Baur SK, Mueller EJ, Huse DA. 2007. *Phys. Rev. Lett.* 99:250403
138. Zhang SC. 1998. *Journal of Physics and Chemistry of Solids* 59:1774
139. Raczkowski M, Capello M, Poilblanc D, Frésard R, Oleś AM. 2007. *Phys. Rev. B* 76:140505
140. Capello M, Raczkowski M, Poilblanc D. 2008. *Phys. Rev. B* 77:224502
141. Loder F, Kampf AP, Kopp T. 2010. *Phys. Rev. B* 81:020511
142. Wårdh J, Granath M. 2017. *Phys. Rev. B* 96:224503
143. Wårdh J, Andersen BM, Granath M. 2018. *Phys. Rev. B* 98:224501
144. Lee SS, Lee PA, Senthil T. 2007. *Phys. Rev. Lett.* 98:067006
145. Soto-Garrido R, Fradkin E. 2014. *Phys. Rev. B* 89:165126
146. Wu C, Sun K, Fradkin E, Zhang SC. 2007. *Phys. Rev. B* 75:115103
147. Soto-Garrido R, Cho GY, Fradkin E. 2015. *Phys. Rev. B* 91:195102
148. Granath M, Oganessian V, Kivelson SA, Fradkin E, Emery VJ. 2001. *Physical Review Letters* 87:167011
149. Sikkema AE, Affleck I, White SR. 1997. *Phys. Rev. Lett.* 79:929
150. Zachar O, Tsvelik AM. 2001. *Phys. Rev. B* 64:033103
151. Zachar O. 2001. *Phys. Rev. B* 63:205104
152. Berg E, Fradkin E, Kivelson SA. 2010. *Phys. Rev. Lett.* 105:146403
153. Cho GY, Soto-Garrido R, Fradkin E. 2014. *Phys. Rev. Lett.* 113:256405
154. Jaefari A, Fradkin E. 2012. *Phys. Rev. B* 85:035104
155. Huang EW, Mendl CB, Jiang HC, Moritz B, Devereaux TP. 2018. *npj Quantum Materials* 3:22
156. Verstraete F, Murg V, Cirac J. 2008. *Advances in Physics* 57:143
157. Corboz P, White SR, Vidal G, Troyer M. 2011. *Phys. Rev. B* 84:041108
158. Corboz P, Rice TM, Troyer M. 2014. *Phys. Rev. Lett.* 113:046402
159. Dodaro JF, Jiang HC, Kivelson SA. 2017. *Phys. Rev. B* 95:155116
160. Jiang HC, Weng ZY, Kivelson SA. 2018. *Phys. Rev. B* 98:140505
161. Jiang HC, Devereaux T. 2018. Superconductivity in the Hubbard model and its interplay with charge stripes and next-nearest hopping t' . arXiv:1806.01465
162. Xu XY, Law KT, Lee PA. 2018. Pair Density Wave in the Doped $t - J$ Model with Ring Exchange on a Triangular Lattice. arXiv:1811.06538
163. Hartnoll SA, Lucas A, Sachdev S. 2019. *Holographic Quantum Matter*. Cambridge, MA: The MIT Press
164. Flauger R, Pajer E, Papanikolaou S. 2011. *Phys. Rev. D* 83:064009
165. Cremonini S, Li L, Ren J. 2017. *Journal of High Energy Physics* 2017:81
166. Cremonini S, Li L, Ren J. 2017. *Phys. Rev. D* 95:041901
167. Cai RG, Li L, Wang YQ, Zaanen J. 2017. *Phys. Rev. Lett.* 119:181601
168. Chandrasekhar BS. 1962. *Applied Physics Letters* 1:7
169. Clogston AM. 1962. *Phys. Rev. Lett.* 9:266–267
170. Sarma G. 2002. *Journal of Physics and Chemistry of Solids* 24:1029
171. Carlson J, Reddy S. 2005. *Phys. Rev. Lett.* 95:060401
172. Regal CA, Jin DS. 2003. *Phys. Rev. Lett.* 90:230404
173. Nikolić P, Sachdev S. 2007. *Phys. Rev. A* 75:033608
174. Veillette MY, Sheehy DE, Radzihovsky L. 2007. *Phys. Rev. A* 75:043614
175. Nishida Y, Son DT. 2006. *Phys. Rev. Lett.* 97:050403
176. Alford M, Bowers JA, Rajagopal K. 2001. *Phys. Rev. D* 63:074016
177. Bowers JA, Rajagopal K. 2002. *Phys. Rev. D* 66:065002
178. Machida K, Nakanishi H. 1984. *Phys. Rev. B* 30:122
179. Burkhardt H, Rainer D. 1994. *Annalen der Physik* 506:181–194
180. Matsuo S, Higashitani S, Nagato Y, Nagai K. 1998. *Journal of The Physical Society of Japan* 67:280–289
181. Yoshida N, Yip SK. 2007. *Phys. Rev. A* 75:063601
182. Mora C, Combescot R. 2005. *Phys. Rev. B* 71:214504
183. Sheehy DE, Radzihovsky L. 2007. *Phys. Rev. B* 75:136501
184. Su WP, Schrieffer JR, Heeger AJ. 1979. *Phys. Rev. Lett.* 42:1698–1701
185. Orso G. 2007. *Phys. Rev. Lett.* 98:070402
186. Hu H, Liu XJ, Drummond PD. 2007. *Phys. Rev. Lett.* 98:070403
187. Yang K. 2001. *Phys. Rev. B* 63:140511
188. Zhao E, Liu WV. 2008. *Phys. Rev. A* 78:063605
189. Radzihovsky L. 2012. *Physica C: Superconductivity* 481:189–206
190. Shimahara H. 1998. *Journal of the Physical Society of Japan* 67:1872–1875
191. deGennes PG, Prost J. 1993. *The Physics of Liquid Crystals*. Oxford, UK: Oxford University Press, 2nd ed.
192. Chaikin PM, Lubensky TC. 1995. *Principles of Condensed Matter Physics*. Cambridge, UK: Cambridge University Press
193. Grinstein G, Pelcovits RA. 1981. *Phys. Rev. Lett.* 47:856–859
194. Agterberg DF, Kaur RP. 2007. *Phys. Rev. B* 75:064511
195. Dimitrova O, Feigel'man MV. 2007. *Phys. Rev. B* 76:014522
196. Gor'kov LP, Rashba EI. 2001. *Phys. Rev. Lett.* 87:037004

197. Frigeri PA, Agterberg DF, Koga A, Sigrist M. 2004. *Phys. Rev. Lett.* 92:097001
198. Cho GY, Bardarson JH, Lu YM, Moore JE. 2012. *Phys. Rev. B* 86:214514
199. Barzykin V, Gor'kov LP. 2002. *Phys. Rev. Lett.* 89:227002
200. Agterberg D. 2002. *Physica C* 387:13
201. Smidman M, Salamon M, Yuan H, Agterberg D. 2017. *Reports on Progress in Physics* 80:036501
202. Hart S, Ren H, Kosowsky M, Ben-Shach G, Leubner P, et al. 2016. *Nature Physics* 13:87 EP
203. Michaeli K, Potter AC, Lee PA. 2012. *Phys. Rev. Lett.* 108:117003
204. Fu L, Kane CL. 2008. *Phys. Rev. Lett.* 100:096407
205. Santos L, Neupert T, Chamon C, Mudry C. 2010. *Phys. Rev. B* 81:184502
206. Chen AQ, Park MJ, Gill ST, Xiao Y, Reig-i Plessis D, et al. 2018. *Nature Communications* 9:3478
207. Bednik G, Zyuzin AA, Burkov AA. 2015. *Phys. Rev. B* 92:035153
208. Li Y, Haldane FDM. 2018. *Phys. Rev. Lett.* 120:067003
209. Wang Y, Ye P. 2016. *Phys. Rev. B* 94:075115
210. He RH, Tanaka K, Mo SK, Sasagawa T, Fujita M, et al. 2008. *Nature Physics* 5:119 EP –
211. Lee WS, Vishik IM, Tanaka K, Lu DH, Sasagawa T, et al. 2007. *Nature* 450:81
212. Renner C, Revaz B, Genoud JY, Kadowaki K, Fischer Ø. 1998. *Physical Review Letters* 80:149
213. Nie L, Tarjus G, Kivelson SA. 2014. *Proceedings of the National Academy of Sciences* 111:7980
214. Berg E, Altman E. 2007. *Phys. Rev. Lett.* 99:247001
215. Parham S, Li H, Nummy TJ, Waugh JA, Zhou XQ, et al. 2017. *Phys. Rev. X* 7:041013
216. Vishik IM, Lee WS, He RH, Hashimoto M, Hussain Z, et al. 2010. *New Journal of Physics* 12:105008
217. Hashimoto M, Nowadnick EA, He RH, Vishik IM, Moritz B, et al. 2014. *Nature Materials* 14:37
218. Dai Z, Lee PA. 2017. *Phys. Rev. B* 95:014506
219. Kapitulnik A, Kivelson SA, Spivak B. 2019. *Rev. Mod. Phys.* 91:011002
220. Zelli M, Kallin C, Berlinsky AJ. 2012. *Phys. Rev. B* 86:104507
221. Wang L, Vafek O. 2013. *Phys. Rev. B* 88:024506
222. Norman MR, Davis JCS. 2018. *Proceedings of the National Academy of Sciences* 115:5389
223. Li L, Wang Y, Komiya S, Ono S, Ando Y, et al. 2010. *Phys. Rev. B* 81:054510
224. Yu F, Hirschberger M, Loew G, Lawson B, Asaba T, et al. 2016. *PNAS* 113:12667
225. Lee PA. 2019. *Phys. Rev. B* 99:035132